Received: 2 August 2022 | Revised: 17 November 2022 | Accepted: 24 November 2022

DOI: 10.1111/jnc.15737

Journal of Neurochemistry JNC The Official Journal of the International Society for Neurochemistry WILEY

ORIGINAL ARTICLE

Use of metabolic glycoengineering and pharmacological inhibitors to assess lipid and protein sialylation on cells

Petra Kranaster[1,2] | Jonathan Blum[1] | Jeremias E. G. A. Dold[2,3] | Valentin Wittmann[2,3] | Marcel Leist[1,2]

[1]In vitro Toxicology and Biomedicine, Dept inaugurated by the Doerenkamp-Zbinden Foundation, University of Konstanz, Constance, Germany

[2]Konstanz Research School Chemical Biology, University of Konstanz, Constance, Germany

[3]Department of Chemistry, University of Konstanz, Constance, Germany

Correspondence
Marcel Leist and Petra Kranaster, *In vitro* Toxicology and Biomedicine, Dept inaugurated by the Doerenkamp-Zbinden Foundation at the University of Konstanz, Konstanz 78457, Germany.
Email: marcel.leist@uni-konstanz.de; petra.kranaster@uni-konstanz.de

Present address
Jeremias E. G. A. Dold, Berufsschulzentrum Radolfzell, Radolfzell am Bodensee, Germany

Funding information
Deutsche Forschungsgemeinschaft, Grant/Award Number: KoRS-CB; SFB 969-project B05; Doerenkamp-Zbinden Stiftung; EU Horizon 2020 research and innovation program, Grant/Award Number: 964537 (RISK-HUNT3R) 964518 (ToxFree); European Food Safety Authority; the BMBF, Grant/Award

Abstract

Metabolic glycoengineering (MGE) has been developed to visualize carbohydrates on live cells. The method allows the fluorescent labeling of sialic acid (Sia) sugar residues on neuronal plasma membranes. For instance, the efficiency of glycosylation along neurite membranes has been characterized as cell health measure in neurotoxicology. Using human dopaminergic neurons as model system, we asked here, whether it was possible to separately label diverse classes of biomolecules and to visualize them selectively on cells. Several approaches suggest that a large proportion of Sia rather incorporated in non-protein components of cell membranes than into glycoproteins. We made use here of deoxymannojirimycin (dMM), a non-toxic inhibitor of protein glycosylation, and of *N*-butyl-deoxynojirimycin (NBdNM) a well-tolerated inhibitor of lipid glycosylation, to develop a method of differential labeling of sialylated membrane lipids (lipid-Sia) or sialylated *N*-glycosylated proteins (protein-Sia) on live neurons. The time resolution at which Sia modification of lipids/proteins was observable was in the range of few hours. The approach was then extended to several other cell types. Using this technique of target-specific MGE, we found that in dopaminergic or sensory neurons >60% of Sia is lipid bound, and thus polysialic acid-neural cell adhesion molecule (PSA-NCAM) cannot be considered the major sialylated membrane component. Different from neurons, most Sia was bound to protein in HepG2 hepatoma cells or in neural crest cells. Thus, our method allows visualization of cell-specific sialylation processes for separate classes of membrane constituents.

Abbreviations: Ac_4ManNAz, *N*-azidoacetylmannosamine; AM, acetoxymethyl; ANOVA, analysis of variance; AraC, Cytarabin; ATCC, American Type Culture Collection; Az, azide; BDNF, brain-derived neurotrophic factor; BMBF, Bundesministerium für Bildung und Forschung; BrefA, Brefeldin A; BRET, bioluminescence resonance energy transfer; cAMP, dibutyryl cyclic adenosine monophosphate; cat.no., catalog number; CHX, cycloheximide; Ctrl, control; DAPT, (2S)-N-[(3,5-Difluorophenyl)acetyl]-L-alanyl-2-phenyl]glycine 1,1-dimethylethyl ester; DBCO, dibenzocyclooctyne; DMB, 1,2-diamino4,5-methylenedioxybenzene; dMM, deoxymannojirimycin; DMSO, dimethyl sulfoxide; dNM, deoxynojirimycin; DoD, day of differentiation; DPSS, diode-pumped solid-state laser; E8, essential 8 medium; EGF, epidermal growth factor; EndoN, endoneuraminidase N; ER, endoplasmic reticulum; FBS, fetal bovine serum; FGF, fibroblast growth factor; FRET, Förster resonance energy transfer; GaAsP, gallium arsenide phosphide photomultiplier; GAPDH, glyceraldehyde 3-phosphate dehydrogenase; GDNF, recombinant human glial cell derived neurotrophic factor; GlcNAc, *N*-Acetylglucosamine; HeNe, A helium–neon laser; HRP, horseradish peroxidase; Ig, immunoglobulin; ImaEva, image evaluation; iPSCs, induced pluripotent stem cells; kDa, kilodalton; KoRS-CB, Konstanz research school-chemical biology; KSR, knockout serum replacement; LSM, laser scanning microscope; LUHMES, Lund human mesencephalic; MALDI, matrix-assisted laser desorption/ionization; ManNAc, *N*-acetyl-mannosamine; MEM, minimal essential medium; MGE, metabolic glycoengineering; MW, molecular weight; n.s., not significant; NBdNM, *N*-butyldeoxynojirimycin; NCAM, neural cell adhesion molecule; NGF, nerve growth factor; PBS, phosphate-buffered saline; PLO, poly-L-ornithine hydrobromide; PNG, peptide: *N*-glycosidase F; PSA, polysialic acid; RRID, resource research identifiers (see scicrunch.org); RT, room temperature; SDS, sodium dodecyl-sulfate; Sia, sialic acid; SiaV, sialidase from *Vibrio cholerae*; SIM, structured illumination image; SMAD, suppressor of mothers against decapentaplegic; STR, short tandem repeat; SUIKER, program for SUperImposing KEy Regions; TBS, tris-buffered saline; TFA, trifluoroacetic acid; TIFF, tag image file format; Tun, tunicamycin.

Number: NeuroTool; the State Ministry of Baden-Wuerttemberg Germany for Economic Affairs, Labour and Tourism, Grant/Award Number: NAM-Accept

KEYWORDS
confocal imaging, ganglioside, metabolic glycoengineering, neural cell adhesion molecule, neuron, polysialic acid, sialic acid

1 | INTRODUCTION

Metabolic glycoengineering (MGE) is a chemical biology method that allows the visualization of certain sugar residues, for example, sialic acid (Sia) on the cell surface. Both, glycolipids and glycoproteins contribute to the MGE signal, and better methods to distinguish these biomolecule classes are especially desirable in neurochemical research. MGE uses the fact that a precursor of Sia, for example, *N*-acetyl-mannosamine (ManNAc) with a chemical tag (e.g., azide = Az) (ManNAz) can be metabolized by live cells to the corresponding Sia analog (e.g., SiaAz) (Campbell et al., 2007; Dube & Bertozzi, 2003; Wratil et al., 2016). Once on the cell's surface, SiaAz can be reacted with an alkyne group, conjugated to, for example, a fluorescent dye or biotin. As the coupling reaction occurs under mild physiological conditions, it allows subsequent detection of Sia on live cells. MGE has recently been used as a method to study Sia on live neurons (Hayes et al., 2022; Kang et al., 2015; Kranaster et al., 2020). Even though MGE successfully detects most of the total cell membrane sialoglycans, it does not distinguish between sialylated proteins and lipids.

Neurons, like all mammalian cells, display a complex range of lipid and protein-linked oligosaccharides on their surface. The outermost sugar moiety of the oligosaccharides often has a key biological role. For instance, terminal Sia residues are recognized by various lectins. A specific feature of the brain is the formation of polysialic acid (PSA) on proteins (Finne et al., 1983). This structure is composed of up to 200 α2,8-linked Sia residues (Muhlenhoff et al., 1998). Another neurochemical particularity is the high plasma membrane content of Sia-containing glycolipids. Especially the gangliosides, sugar-modified sphingolipids, play a role here. They form a critical component of membrane rafts and influence the functional properties of the neuronal cell membrane (Sipione et al., 2020). As gangliosides carry approximately 75% of the Sia-content of the brain (Schnaar et al., 2014) they are likely to contribute a major proportion of the neuronal MGE-Sia signal.

A particularly important Sia-modified brain protein is neural cell adhesion molecule (NCAM). This cell surface glycoprotein belongs to the immunoglobulin superfamily (Aonurm-Helm et al., 2016; Hoffman et al., 1982). Different NCAM isoforms can be generated by alternative mRNA splicing (Goridis & Brunet, 1992): the membrane isoforms have a molecular weight of 120, 140, and 180 kDa, while proteolytically processed cytosolic isoforms have 105–115 kDa (Kiselyov et al., 2005). Moreover, polysialylation of NCAM can account for up to 30% of its relative molecular mass (Bonfanti, 2006).

Many alternatives to MGE are available to analyze sialoproteins and sialolipids. Matrix-assisted laser desorption/ionization (MALDI) mass spectrometry (Jackson et al., 2007; Sarbu et al., 2022), chromatography, colorimetry, fluorometry, and/or enzymatic analysis (Rudd et al., 2021) have been applied to cell lysates. Also, selective release of Sia from complex glycans and their subsequent reaction with 1, 2-diamino-4,5-methylenedioxybenzene (DMB) has been abundantly used to generate fluorescent compounds measured by high-pressure liquid chromatography (Dold & Wittmann, 2021). Sia-lipids and Sia-proteins have been detected on fixed cells or tissue samples by lectins or antibodies (Goodfellow & Willison, 2016; Lopes, 2019; Porter et al., 2021; Wright & Andrews, 2009). However, information on real-time distribution of sialoglycoconjugates on the membrane of live neurons is difficult to obtain with these methods.

Removal of sialoglycoconjugates from cellular surfaces by cleavage of different glycosidic linkages via the use of enzymes has been used to increase the specificity of detection methods. For instance, protein N-glycosidase F (PNG) cleaves the amide linkage between GlcNAc and asparagine residues from N-linked glycoproteins (Maley et al., 1989) and different sialidases catalyze the hydrolysis of Sia residues from glycoproteins and glycolipids. However, because of their significant cytotoxic effects, application of these enzymes as sialylation modulators of live neurons is not ideal.

Inhibitors of glycosidases are interesting new tools that may be used in combination with analytical methods to study glycosylation. Several of these compounds have been developed as drugs for lipid storage diseases. Thus, there is a wealth of information on their good cellular uptake and tolerability. Most drug-like compounds have been derived from imino sugars that are found in plants (Butters et al., 2005; Fleet et al., 1990; Gruters et al., 1987). For instance, the mannosidase inhibitor deoxymannojirimycin (dMM) has been successfully used to inhibit the trimming reactions of N-linked protein glycoconjugates. Inhibition of carbohydrate trimming is known to prevent sialylation of glycoproteins and instead leads to proteins with a high content of mannose in their terminal sugars. The antiviral drugs castanospermine and deoxynojirimycin (dNM) are glucosidase inhibitors. Alkylation of such compounds can change their properties. For instance, *N*-butylation of dNM (NBdNM) converts it into an inhibitor of ceramide-specific glucosyltransferase, and thus prevents ganglioside biosynthesis (Butters et al., 2000; Platt & Butters, 1998; Platt et al., 1994; Shayman, 2013). Imino sugar-derived drugs could therefore offer a possibility to selectively inhibit the sialylation of either proteins or lipids.

We hypothesized here, that the high content of sialylated lipids in the brain would cause the MGE signal on neurons to be of little specificity for glycoproteins. We reasoned that this may even be the case if polysialylation of, for example, NCAM is taken into account. This would mean that studies based mainly on MGE to follow neuronal glycoproteins (Kang et al., 2015) would need to be re-interpreted. We tested our hypothesis by examining the effect of compounds that affect glycoproteins on the MGE Sia signal of cultured neurons. We explored whether and how specific

inhibition of the MGE signal by dMM and NBdNM would affect protein and lipid sialylation. Finally, we applied the differential inhibition approach to several cell types, ranging from hepatoma cells to peripheral neurons.

2 | MATERIALS AND METHODS

2.1 | Cell culture

2.1.1 | LUHMES neurons

LUHMES cells (RRID:CVCL_B056; ATCC number: CRL-2927) were cultured as previously described (Chovancova et al., 2017; Delp et al., 2019; Gutbier, May, et al., 2018; Gutbier, Spreng, et al., 2018; Kranaster et al., 2020; Scholz et al., 2011, 2018). No institutional ethical approval was required for this exploratory study using standard cell lines. Cells were fully characterized and short tandem repeat (STR) authenticated (Gutbier, May, et al., 2018). Plastic cell culture flasks (cat. no. 83.3911.002; Sarstedt) and plates (cat.no. 83.3920) were pre-coated with 50 μg/ml Poly-L-ornithine (cat. no. P3655-10MG) and 1 μg/ml fibronectin (cat.no. F1141) (both from Sigma-Aldrich) in H_2O overnight. For microscopy experiments, 8-well glass bottom ibidi slides (cat.no. 80807; Ibidi) were used and 1 mg/ml laminin (cat.no. L4544; Sigma Aldrich) was added to the standard coating solution. After removal of coating solution, flasks, plates or slides were washed once with H_2O and air-dried before cell seeding. LUHMES cells were cultured at 37°C in a humidified 95% air with 5% CO_2 atmosphere.

Proliferation medium contained: Advanced Dulbecco's modified Eagle's medium/F12 (cat.no. 12634028; Thermo Fisher Scientific), supplemented with 1× N-2 supplement (cat.no. 17502048; Thermo Fisher Scientific), 2 mM L-glutamine (cat.no. G7513; Sigma Aldrich) and 40 ng/mL recombinant human basic FGF (cat.no. 4114-TC; R&D Systems). For maintenance, proliferating cells were dissociated using trypsin (cat.no. 25300054; Thermo Fisher Scientific) every 2–3 days. Maximum passage number for the cells was 18.

Differentiation medium contained: Advanced Dulbecco's modified Eagle's medium/F12, supplemented with 1× N-2 supplement, 2 mM L-glutamine, 1 mM dibutyryl cAMP (cat.no. D0627-1G; Merck), 1 μg/mL tetracycline (cat.no. T-7660; Merck) and 2 ng/ml recombinant human GDNF (cat.no. 212-GD; R&D Systems). To start the differentiation, 8×10^6 LUHMES were seeded into a T175 flask in the proliferation medium. After 24 h, differentiation was initiated (=day 0 of differentiation), by changing of proliferation medium for differentiation medium. After 2 days of cultivation in culture flasks (=day 2 of differentiation), cells were trypsinized and seeded into the pre-coated 96-well plates (for cytotoxicity experiments), in 8-well glass bottom ibidi μ-slides (for confocal imaging) or in 6-well plates (for Western blot analysis and 1,2-diamino-4,5-methylenedioxybenzene (DMB) labeling of Sia) at the density of 150,000 cells/cm^2.

2.1.2 | Peripheral neurons

Peripheral neurons were differentiated from induced pluripotent stem cells (iPSCs) and frozen exactly as described (Holzer et al., 2022). In brief, the human iPSC line SBAD2 (RRID:CVCL_ZX54) (Chen et al., 2011) was predifferentiated into immature sensory neurons in 100% KSR medium (knockout serum replacement DMEM; cat.no. 10829018) supplemented with 15% serum replacement (cat. no. 10828010), 1×Glutamax (cat.no. 35050061), 1×non-essential amino acids (cat.no. 11140050), and 50 μM βmercaptoethanol (cat. no. 31350010) (all from Thermo Fisher Scientific) using dual SMAD inhibition and small molecule inhibitors addition: noggin (cat.no. 6057-GMP; R&D Systems) (17.5 ng/ml), SB431542 (10 μM) (cat.no. 1614; Tocris) and dorso (cat.no.3903; Tocris) (600 nM). After 9 days, the immature neurons were frozen in 90% fetal bovine serum (FBS) (cat.no.10082147; Thermo Fisher Scientific) and 10% dimethyl sulfoxide (DMSO, cat.no. D1435 Merck). After thawing of the predifferentiated cells, neuron precursors were cultured in 25% KSR and 75% N2-S supplemented with CHIR99021 (cat.no. 1386; Axon Medchem) (1.5 μM), SU5402 (cat. no. 3300; Tocris) (5 μM) and DAPT (cat.no. 2634/10; Tocris) (5 μM). 100,000 cells/cm^2 were seeded on MatrigelTM (cat.no. 734-0270; VWR) coated 8-well ibidi slides. On DoD1 and DoD2, half medium exchange was performed and on DoD2, Matrigel was also added at a final dilution of 1:80. On DoD3, medium was replaced by N2-S medium (DMEM/F12, 1×GlutaMax supplemented with 12.5 ng/ml brain-derived neurotrophic factor; BDNF; cat.no. 248-BDB), 25 ng/ml glia-derived neurotrophic factor (GDNF; cat. no. 212-GMP) and 25 ng/ml nerve growth factor (NGF; cat. no. 256-GF) (all from Bio-Techne) and 2 μM cytarabin (AraC; cat.no. C3350000 Merck). Cells were fully characterized and STR authenticated (Holzer et al., 2022). Cells were treated with test compounds on DoD0 or DoD4 and analysis was performed on 24 h later.

2.1.3 | HepG2 hepatoma cells

The human HepG2 cells (RRID:CVCL_A8FT; ATCC number HB-8065) were cultured in 5% CO_2 at 37°C in RPMI 1640 medium (cat. no. 11875093; Thermo Fischer Scientific) supplemented with 10% (v/v) fetal calf serum. Cells were subcultured every 3–4 days and seeded onto uncoated Sarstedt 6-well plates (for Western blot experiments) or coated ibidi slides (for microscopy experiments) at a density of 0.2×10^5 cells/cm^2. Maximum passage for the cells was 10.

2.1.4 | Neural crest cells

Neural crest cells were differentiated from the induced pluripotent stem cell (iPSC) line IMR90_clone_#4 (RRID:CVCL_C436; WiCell) exactly as described earlier (Dolde et al., 2021). To initiate differentiation in neural crest cells, iPSCs were plated on MatrigelTM coated 6-well plates at a density of 100,000 cells/cm^2 in E8 medium (cat.no. A2656101; Thermo Fisher Scientific) containing

10 μM ROCK inhibitor (Y-27632; cat. no. 1254; Tocris). 24 h later (=day 0 of differentiation), when cells were about 70%–80% confluent, the medium was exchanged for KSR medium (knockout DMEM, 15% knockout serum replacement, 1% GlutaMax, 1% MEM NEAA solution, and 50 μM 2-mercaptoethanol supplemented with 20 ng/ml noggin and 10 μM SB431542; cat. no. 1614/1; Tocris). From day 2 of differentiation, cells were treated with 3 μM CHIR 99021. Noggin and SB431542 were taken out of the medium at days 3 and 4 of differentiation, respectively. From day 4, the KSR medium was gradually replaced by 25% enhancements of N2-S medium (DMEM/F12, 1% GlutaMax, 1.55 mg/ml glucose; cat. no. Y0001745), 0.1 mg/ml apotransferin (cat. no. 616419-M), 25 μg/ml insulin (cat. no. I9278), 20 nM progesterone (cat. no. P8783), 100 μM putrescine (cat. no. 51799), and 30 nM selenium (cat.no. NIST3149) (all from Merck). On day 11, cells were resuspended in N2-S medium supplemented with 20 ng/ml EGF (cat. no. 236-GMP) and 20 ng/ml FGF2 (cat. no. 3718-FB) (both from R&D Systems) and seeded as droplets (10 μl) on poly-L-ornithine (PLO)/laminin/fibronectin-coated 10 cm dishes. Cells were weekly passaged and the medium was changed every second day. After 35–39 days, cells were frozen in 90% N2-S medium and 10% dimethyl sulfoxide (DMSO). Cells were then freshly thawed on the day of the experiment. 95,000 cells/cm^2 were seeded on poly-L-ornithine/fibronectin/laminin-coated 8-well ibidi slides or 6-well plates in N2-S medium supplemented with 20 ng/ml EGF and 20 ng/ml FGF2. One hour after seeding, cells were treated with test compounds and analysis was performed 24 h after.

None of the cell lines used in this study are listed as commonly misidentified cell lines by the International Cell Line Authentication Committee (ICLAC; http://iclac.org/databases/cross-contaminations/).

2.2 | MGE to label cell surface sialic acids

Ac_4ManNAz was synthetized according to the published procedures (Saxon & Bertozzi, 2000; Saxon et al., 2002). A stock solution (100 mM) was prepared and stored at −20°C until use. On the day of experiment, working solution was prepared by diluting the stock solution in cell culture medium. The corresponding volume of dimethyl sulfoxide (DMSO) in medium was used as a control. After the treatment with the sugar derivative Ac_4ManNAz, cells were washed twice with PBS. The azide tag was then reacted for 20 min with dibenzocyclooctyne-PEG_4-biotin (DBCO-biotin) (cat. no. CLK-A105P4-10 Jena Bioscience) (100 μM) at 37°C.

The DBCO-biotin labeled cells were incubated with a mixture of streptavidin-Alexa Fluor 488 (8 μg/ml) (cat. no. S11223 Thermo Fisher Scientific) and H-33342 (1 μg/ml) (cat. no. H1399; Thermo Fisher Scientific) for 20 min at 37°C in the dark. For the neurite area recognition, CellTrace™ Calcein Red–Orange (10 μM) (cat. no. C34851; Thermo Fischer Scientific) was added to the staining mixture. Cells were then washed twice with PBS and either imaged live or fixed with 2% paraformaldehyde containing (cat.no. J61899.AK; Thermo Fisher Scientific) 4% sucrose (cat.no. A15583.36; Thermo Fisher Scientific) for 10 min at room temperature (RT) in the dark. Afterward, cells were thrice washed and stored in PBS at 4°C in the dark until imaging.

2.3 | Confocal and high resolution fluorescence microscopy

Cells were imaged using a Zeiss LSM 880 point laser scanning confocal microscope equipped with GaAsP detector and a 40×/1.40 PlanApochromat oil immersion objective (Zeiss) was used. Lasers HeNe (633 nm), diode-pumped solid-state (DPSS) (561 nm), Argon (458, 488, 514 nm), and Diode 405-30 (405 nm) were used. If not otherwise indicated, five images were taken per condition as a z-stack images, by defining a bottom slice and imaging nine focal planes with a 0.5 μm distance in between, with a total z-range of 4 μm. Fiji software (Rueden et al., 2017) was used to convert the images into maximum z-stack projections. Images were quantified using the SUIKER program (Karreman et al., 2019), freely accessible at https://invitrotox.uni-konstanz.de/Suiker/.

High resolution images were taken using the Deltavision OMX (GE Healthcare) equipped with 60× objective (numerical aperture 1.42) and the laser lines 488 and 405 nm were used. Raw SIM images were reconstructed using the Softworx OMX image reconstruction algorithm. Multichannel images imaged on separate cameras were aligned using reference images created with the Deltavision image registration sample.

2.4 | Immunocytochemistry

Cells on pre-coated 8-well glass bottom ibidi slides were treated with Ac_4ManNAz. MGE labeling was performed as described above. Afterwards, the cells were fixed as described above. The slides were washed and pre-incubated with PBS/1% bovine serum albumin (cat. no. 2905-OP; Merck) for 1 h at 21°C. Primary mouse anti-PSA IgM antibody (RRID:AB_95211; Merck) diluted 1:400 in PBS containing 2% fetal bovine serum or primary rabbit anti-NCAM IgG antibody (RRID:AB_10804456; Merck) diluted 1:500 in PBS 2% fetal bovine serum was added for 1 h at 21°C. Slides were then washed three times with PBS and secondary rabbit AlexaFluor555 (RRID:AB_2535849; Thermo Fisher Scientific) or secondary mouse AlexaFluor647 (RRID:AB_162542; Thermo Fisher Scientific) (diluted 1:1000 in 2% FCS PBS) was applied as secondary antibody for 1 h at 21°C. Prior to the next washing step, H-33342 (1 μg/ml) was added for 10 min. Samples were imaged same as described above.

2.5 | SDS-page and Western blot

Cells were lysed in 1 × Laemmli buffer and boiled at 95°C for 5 min. To remove long strands of DNA, lysates were centrifuged for 1 min

at 10000×*g* using NucleoSpin Filters (cat.no. 740606 Macherey-Nagel, Germany). Thirty-five microgram of total protein were loaded on 10% SDS gels after which proteins were transferred onto nitrocellulose membranes (cat. no. LC2000; Thermo Fisher Scientific) using the iBlot 2 Dry Blotting System (Thermo Fisher Scientific). The membranes were blocked with 5% milk (w/v) in TBS-Tween (0.1% [v/v]) (cat. no. 28360; Thermo Fisher Scientific) for 1 h. Anti-glyceraldehyde 3-phosphate dehydrogenase (GAPDH) mouse antibody ZG003 (1:10000) (RRID:AB_2533438; Thermo Fisher Scientific), anti-biotin mouse antibody HRP (1:1000) (cat. no. 7075 S; Cell Signaling Technology), anti-PSA NCAM mouse antibody clone 2-2B or anti-NCAM rabbit antibody were used as primary antibodies. They were diluted in 2% milk (w/v) in TBS-Tween (0.1% [v/v]) and added onto the membranes and incubated at 4°C overnight. Membranes were washed three times for 10 min with TBS-Tween (0.1%). Then, peroxidase AffiniPure goat anti-mouse (1:10000) (RRID:AB_2338512; Jackson Immunoresearch) or donkey anti-rabbit NA934V IgG (1:10000) (RRID:AB_772206; Cytiva) secondary antibodies diluted in 2% milk (w/v) in TBS-Tween (0.1% [v/v]) were added for 1 h at RT. After three further 10 min washes with TBS-Tween (0.1%), ECL western blotting substrate (cat. no. 32106; Thermo Fisher Scientific) was used for visualization. Quantification of the relative band/lane intensity was performed using a self-developed Image Evaluation (ImaEva) program and the intensities were normalized to the corresponding GAPDH loading control. The program ImaEva quantifies the intensity of the Western Blot bands and lanes. The pictures are uploaded into the program in 16-bit TIFF format, usually with a 512×512 pixel resolution. The program shows an enhanced version of the image for easier manipulation, however, all calculations are performed with the original TIFF files' pixel values. Bands or regions of interest in each image are then selected and surrounded by an arbitrary shape. The total chemo-luminescence signal within the selected shape is then calculated. Background correction is performed by the selection of a single relevant area. The pixel values are then exported directly into an Excel file. If not otherwise stated, at least three blots from three independent cell culture preparations were quantified. The original Western blot images can be found in Figure S8.

2.6 | Inhibition of sialylation

Compounds were prepared from the following stock solutions: cycloheximide (7 mM in DMSO; cat. no. 239764) tunicamycin (10 mM in DMSO; cat. no. T7765), brefeldin A (35 mM in DMSO; cat. no. B6542), deoxymannojirimycin (100 mM in H_2O; cat. no. D9160), swainsonine (290 mM in H_2O; cat. no. S9263) (all from Merck); and castanospermine (cat. no. 0759) and *N*-butyl deoxynojirimycin (cat. no. 3117) (both as 100 mM in H_2O) (both from Tocris). If not otherwise stated, cells were treated with inhibitors diluted from stock solution into media for 24 h.

2.7 | Enzymatic removal of sialoglycoconjugates

Enzymatic treatment was performed with differentiated LUHMES cells on day 6 by adding 2500 U protein N-glycosidase F (PNG; cat. no. P0704L; New England Biolabs), 40U endoneuraminidase N (EndoN; cat. no. AbC0020; Linaris biologische Produkte), or 200 U sialidase from *Vibrio cholerae* (siaV; cat. no. N6514; Merck) for 2 h at 37°C. After incubation, the cells were washed twice with PBS and used for further experiments.

2.8 | Quantification of neurite viability by high content imaging

LUHMES cells were differentiated for 2 days and seeded in 96-well plates at a density of 150,000 cells/cm^2 in a volume of 90 µl of differentiation medium. Test compounds were added on day 5 of differentiation as 10 µl from a 10× concentrated solution. The assay was based on the previously described method (Stiegler et al., 2011). A staining solution, consisting of 1 µM calcein-AM (cat.no. C3099; Thermo Fisher Scientific) and 1 µg/ml H-33342 was added to the wells for 30 min at 37°C. An automated microscope Array-Scan VTI HCS Reader (Thermo Fisher Scientific) was used for imaging. Channel 1 (365 ± 50/461 ± 15 nm) recorded the nuclei staining and channel 2 (475 ± 40/525 ± 15 nm) the calcein. The neuronal somatic area was then identified based on an algorithm using the object size, area, and intensity from channel 1. The neurite area was then identified by expansion of the neuronal somatic area and its subtraction from the calcein area. H-33342 and calcein-positive cells were detected as live, whereas cells positive for H-33342 only were identified as dead. Both live cells and neurite area were expressed as percentage relative to the (solvent-treated cells) control.

2.9 | Quantification of MGE by SUIKER program

The program for SUperImposing KEy Regions (SUIKER) was applied for the simultaneous quantification of viability, neurite area, and MGE sugar incorporation into neurites. The confocal microscopy images were firstly processed into the z-stack maximum projection images using Fiji. Afterwards, the images were imported into SUIKER. Using the fluorescent channels' information, the software then detected the nucleus in the blue channel, the cytoplasm in the green channel, and the MGE-labeled Sia in the red channel. Nuclei were counted in the blue channel based their somatic area and exclusion of any background fluorescence as well as nuclear debris. By size exclusion of the small non-viable nuclei, the viability was determined. Neurite area was then recorded and quantified by subtracting the soma area from the green cytoplasmic channel. The neurite MGE intensity was measured as the pixel intensities from the red channel within the neurite area. The software outputs, exported as Microsoft Excel file, were analyzed using

GraphPad Prism. The SUIKER program is freely accessible at https://invitrotox.uni-konstanz.de/Suiker/.

2.10 | Measurement of the Sia incorporation efficiency by 1,2-diamino-4,5-methylenedioxybenzene labeling

LUHMES cells were seeded on day 2 of differentiation on pre-coated 6-well plates at the density of 150000 cells/cm^2. Tested compounds or the corresponding solvent control were added on day 5 of differentiation. At 24 h later, cells were washed twice with PBS, scraped-off the well surface, and pelleted. The release of Sia and DMB labeling was performed as previously described (Dold et al., 2017) using standard chemicals (all purchased from Merck). The cell pellets were resuspended in 300 µl AcOH (3 M) to release the Sia, and the mixture was incubated for 90 min at 80 °C inside a thermomixer at 300 rpm. The mixtures were diluted in 400 µl water. To neutralize the solution, 20 µl of 25% NH_3 in water was added. SpeedVac was used to remove the solvent, and each pellet was washed with 200 µl EtOH three times after each step. The pellets were then resuspended in 265 µl DMB labeling solution containing 5.3 mM DMB·2 HCl, 16 mM $Na_2S_2O_4$, 40 mM trifluoroacetic acid (TFA) in MilliQ water and incubated for 2.5 h at 56°C inside a thermomixer at 300 rpm in the dark. The mixture was then cooled for 10 min on ice. For neutralization, 25 µl of aqueous NaOH (0.5 M) was used. RP–HPLC–MS with additional fluorescence detection (λ_{ex} = 372 nm, λ_{em} = 456 nm) was used to analyze the samples.

2.11 | Data analysis and statistics

No animals were used in this exploratory study and no preregistration was submitted. Statistical differences were tested by one-way ANOVA followed by Dunnett's multiple comparisons test, using GraphPad Prism 7.04 (GraphPad Software). Statistical reports are included in the figure legends and in Figure S9. Observer blinding was not used as all quantitative data were obtained by unbiased methods (automatic imaging algorithms). Sample size calculations can be found in Figure S10. The data are presented as means of at least three independent biological replicates (i.e., using three different cell preparations, unless stated otherwise). Data were not assessed for normality and no test for outliers was conducted. No exclusion criteria were pre-determined in our study and no samples were excluded or replaced.

3 | RESULTS

3.1 | Experimental strategy

The brain is particularly rich in sialylated glycolipids. On this basis we were astonished to see that, in some publications, neuronal surface glycosylation, as detected by MGE, was considered to be caused only (or mainly) by glycoproteins (Kang et al., 2015). We investigated this issue here by several approaches: (i) First we used relatively unspecific tools to inhibit protein glycan formation and to check the effect on MGE-Sia detection on neurons; (ii) then, we investigated claims (Kang et al., 2015) that NCAM sialylation was the major component of the MGE signal on neurons; (iii) finally, we developed a specific method to only stain sialolipids or sialoproteins.

3.2 | Preliminary exploration of the role of proteins in neuronal surface sialylation

As first step of our strategy, we explored several approaches to investigate the extent to which Sia-MGE signals are linked to protein glycans. For this purpose, several compounds known to interfere with protein synthesis and processing were tested. In pilot studies, the concentrations tolerated by neurons were determined and cytotoxicity thresholds were defined: Mature central nervous system LUHMES neurons were treated with increasing concentrations of the inhibitors for 24 h, and the percentages of live cells and of the neurite area were quantified by high content imagining (Figure 1a). The protein synthesis inhibitor cycloheximide (CHX) was cytotoxic at concentrations >3.6 µM (more than 25% loss of neurite area). The antibiotic tunicamycin (Tun), known to inhibit N-glycosylation of proteins (nearly completely shuts down the synthesis of glycans required for transfer to glycosylated proteins at 10–100 nM; Ko et al., 2020), was cytotoxic at concentrations >100 nM. Brefeldin A (BrefA)—is known to impair transport from ER to Golgi. It fully blocks membrane incorporation of glycosylated proteins and lipids at low micromolar concentrations (Kaczmarek et al., 2017; Maccioni et al., 2011; van Echten et al., 1990). Onset of cytotoxicity was observed at submicromolar concentrations, but then, a stable plateau was reached with about 70% of neurons and neurites surviving. A concentration of 3.6 µM was chosen for further experiments (Figure 1b).

For the main experimental approach, we labeled LUHMES Sia residues with a MGE approach (Kranaster et al., 2020): Cells were fed with a Sia precursor (peracetylated *N*-azidoacetylmannosamine = Ac_4ManNAz) that is known to be incorporated into neuronal sialoglycans. These sugars were labeled with a fluorescent tag on live neurons via a bioorthogonal ligation (=MGE-Sia signal). At the same time, the neurons were co-treated with the inhibitor (at concentrations determined before to allow neuronal survival, but to shut down various pathways involved in the processing of glycoproteins). Then, the MGE signal intensity was measured: After the inhibition of protein synthesis with CHX, about half of the MGE signal was still observed. The same was found for cells treated with Tun. In the case of BrefA treatment, only 9% of neurite MGE was detected (Figure 1c).

Altogether, these data suggest that sialoproteins only partially contribute to the neuronal surface sialylation. The strong effect of BrefA, which inhibits the translocation of both lipids and proteins, provided circumstantial evidence that sialolipids take a major role.

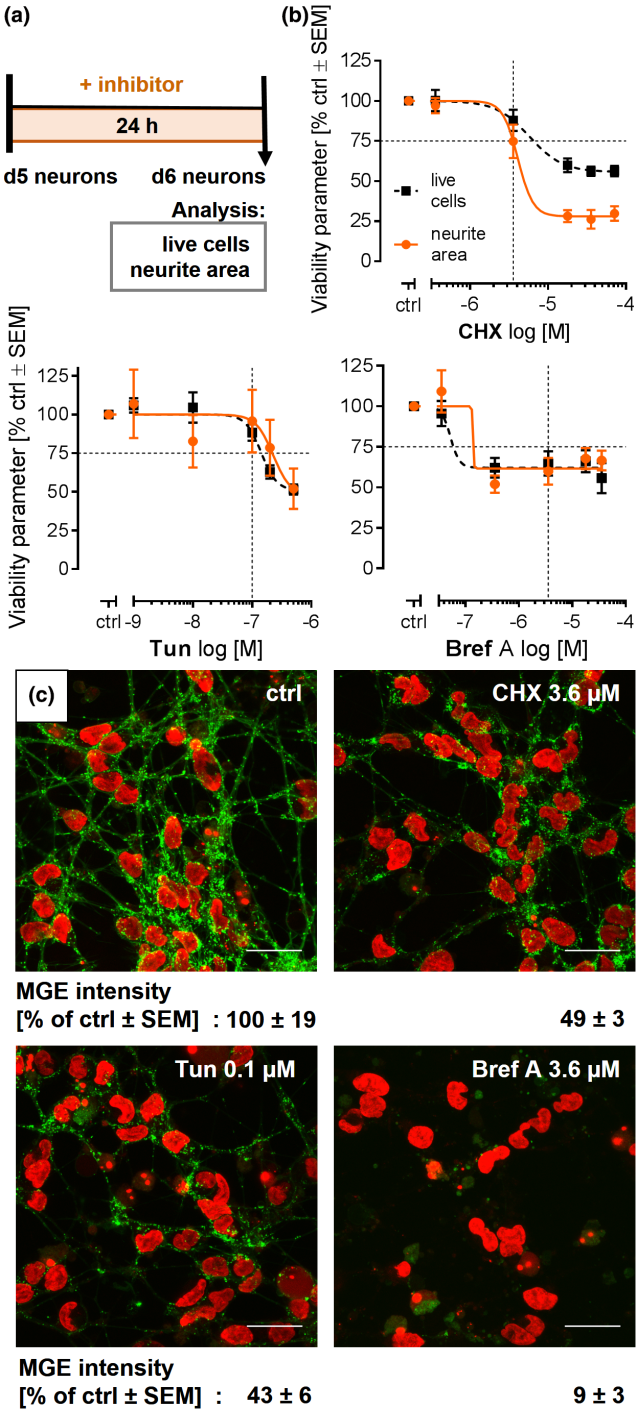

FIGURE 1 MGE Sia levels after unspecific inhibition of sialoglycan synthesis. (a) Schematic representation of the cytotoxicity assay. LUHMES neurons differentiated for 5 days (d5) were treated with inhibitors for 24 h and their viability was determined by high content imaging using H-33342/calcein-AM staining. (b) Concentration–response curves indicate the percentage of live cells (dashed line) and of the neurite area (solid line), relative to the untreated cells. The horizontal line is drawn at 75% (toxicity threshold). The vertical dotted line indicates the concentration selected for metabolic glycoengineering (MGE) sialic acid (Sia) labeling in (c). (c) Representative confocal fluorescent images of MGE Sia (green) and nuclei (red) of day 6 (d6) LUHMES cells treated for 24 h with indicated concentrations of cycloheximide (CHX), tunicamycin (Tun), or brefeldin a (Bref a). The level of MGE Sia was quantified by an imaging algorithm, and it is indicated below each image as the percentage of untreated control (ctrl). Data are presented as means from three independent biological replicates (=three independent cell preparations). Scale bar = 25 µm.

3.3 | Examining the role of PSA-NCAM for neuronal cell membrane sialic acid content

As second step of our strategy, we investigated claims in the literature that NCAM glycosylation accounted for the majority of the Sia-MGE signal. First, we examined whether there was at all a correlation of NCAM expression and Sia-MGE in various human neuronal cell culture models. As NCAM expression and its polysialylation varies throughout neuronal development and differentiation, and among different neuronal cell types, we first identified at what stage of differentiation our cells express PSA-NCAM. Immature or mature neurons were exposed to the Sia precursor Ac_4ManNAz for 24 h. Then, MGE-Sia was detected by immunostaining, and samples were prepared for Western blotting. In developing LUHMES neurons, we detected only the low molecular weight NCAM-120 isoform, and no polysialylated proteins (Figure 2a). In immature peripheral neurons, no membrane forms of NCAM were detected at all (Figure 2b). Although both cultures of immature neurons were devoid of any signal that would indicate the presence of PSA-NCAM, Sia residues were readily detectable on the cell surfaces by MGE (Figure S1). From this approach we conclude that the neuronal MGE signal can be positive even in the absence of PSA-NCAM. These findings suggest that there are at least some types of neurons/neuronal stages for which PSA-NCAM is not the dominant Sia-carrying membrane constituent.

When we performed similar studies in fully differentiated neurons, the situation was more complex. In both, post-mitotic LUHMES neurons and mature iPSC-derived peripheral neurons, we detected all three membranal NCAM isoforms: NCAM-120, NCAM-140, and NCAM-180 by Western blot (Figure 2a,b, left) Furthermore, NCAM-180 showed a strong level of polysialylation (Figure 2a,b, right). The expression of the polysialylated NCAM in mature LUHMES and peripheral neurons was also confirmed by immunostaining (Figure 2c,d). Taken together, we confirmed the presence of strongly polysialylated-NCAM in the mature stages of our culture models. However, it was not clear, to which extent polysialylation on NCAM contributed to the overall cell surface sialylation. Therefore, we undertook a series of experiments to modify the polysialylation signal in mature, PSA-NCAM expressing, LUHMES cells. As a basis for these studies, Sia on the neuronal surface was labeled with the MGE approach and the same cells were then immunostained for NCAM and PSA. In parallel cultures, the glycan chains of N-glycosylated proteins were removed with PNG (Figure S2). In a second approach, PSA was removed with endoneuraminidase N (EndoN). Both enzyme treatments removed PSA nearly completely from the LUHMES cells' surface (Figure 3a). Quantification of the PSA immunostaining showed that PNG reduced the PSA content by 92%; EndoN had an even

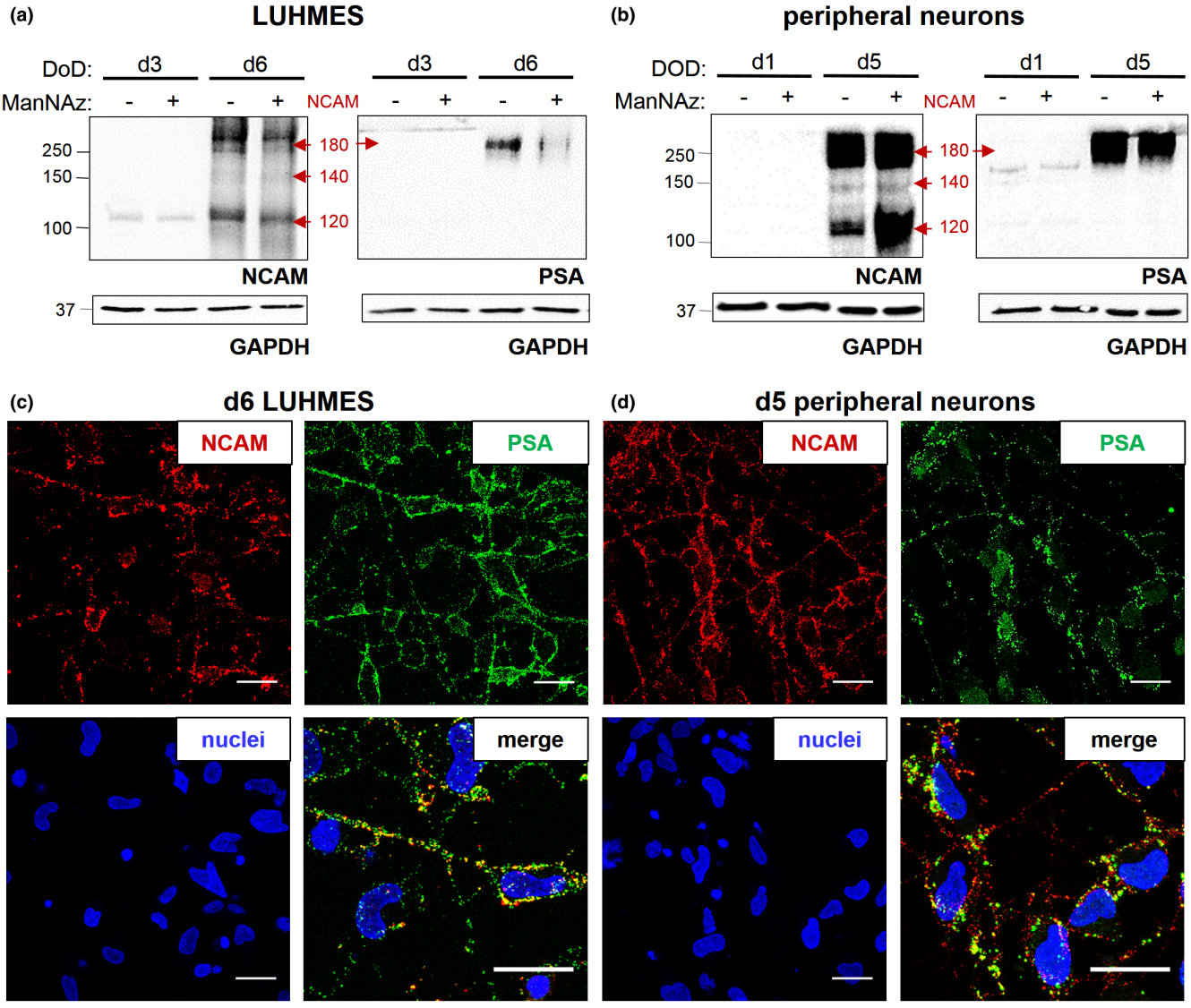

FIGURE 2 Expression of PSA and NCAM in developing and mature neurons. LUHMES cells (central nervous system precursors) were triggered for neuronal differentiation and used after 2 days in culture (d2, immature state) or after 5 days (d5, fully post-mitotic, with extended neurites). Peripheral neurons were differentiated from induced pluripotent stem cells (iPSC) and frozen at the early neural stage. They were used directly after thawing (d0, immature) or 4 days later (d4, fully post-mitotic). Developing (d2 LUHMES, d0 peripheral neurons) and differentiated (d5 LUHMES, d4 peripheral neurons) neurons were cultured for 24 h. note, that during this time, some of the cells (marked with "+") were treated with 10 μM of the sialic acid (Sia) precursor Ac_4ManNAz ("ManNAz") or left untreated ("-"). This showed that the presence of the metabolic glycoengineering (MGE) substrate as such had no effect on neural cell adhesion molecule/polysialic acid (NCAM/PSA) expression. It also gives an overview of reproducibility between "duplicate" samples. Cell lysates were prepared or cells were fixed on d3 and d1 (for developing immature LUHMES and peripheral neurons, respectively) or on d6 and d5 (for mature LUHMES and peripheral neurons, respectively). (a, b) Western blots were performed using anti-NCAM (left) or anti-PSA (right) antibodies; anti-glyceraldehyde 3-phosphate dehydrogenase (GAPDH) was used as a loading control (bottom). The positions of molecular weight markers are indicated on the left. The positions of the three NCAM isoforms (NCAM-180, NCAM-140, and NCAM-120) and indicated by arrows on the right side of the membranes. Note: Polysialylation of NCAM increases its relative molecular weight. The PSA-NCAM bands were present both, in the presence or absence of the Sia precursor sugar (ManNAz). Blots representative of three experiments (from three independent cell culture preparations) are shown. Bands were not quantified, as qualitative information on overall staining patterns was intended. (c, d) Differentiated (day 6) LUHMES cells and (day 5) peripheral neurons were immunostained for NCAM and PSA. Nuclei were counter-stained with H-33342. Images were taken by confocal microscopy, scale bar = 25 μm. Images are representative of three experiments (=three independent cell culture preparations).

stronger (about 100%) effect (Figure 3b). However, the MGE signal was little affected by enzymatic treatments (Figure 3a). When quantified, about 70% of MGE the signal was still present on the neuronal plasma membrane, even when N-glycans or PSA were almost completely removed (Figure 3c).

We conclude that post-mitotic neurons display high NCAM polysialylation, but in LUHMES cells this accounts only for a small proportion of their total cell surface Sia content.

Thus, we found by two approaches (generally blocking glycoprotein synthesis or looking at the example protein NCAM), that there

is a very large component of Sia-MGE not linked to proteins. To better analyze this, we worked on an approach to specifically visualize Sia-lipids.

3.4 | Use of imino sugars for specific inhibition of protein and lipid sialylation in neurons

We wondered whether it was possible to selectively block sialoproteins or sialolipids synthesis under non-toxic conditions. This would allow specific observations of one of the processes on live neurons. On examining potential experimental strategies, we realized that several imino sugars acting as glycosidase inhibitors have been developed for clinical use in lipid storage diseases (Butters et al., 2005). Some of them are known to specifically interfere with either protein or lipid glycosylation processes: Deoxymannojirimycin (dMM) appeared optimal to prevent the incorporation of the newly labeled Sia into glycoproteins; *N*-butyl deoxynojirimycin (NBdNM) was a candidate compound to inhibit the incorporation of Sia into glycolipids (Figure 4a). The effect of these imino sugars was tested

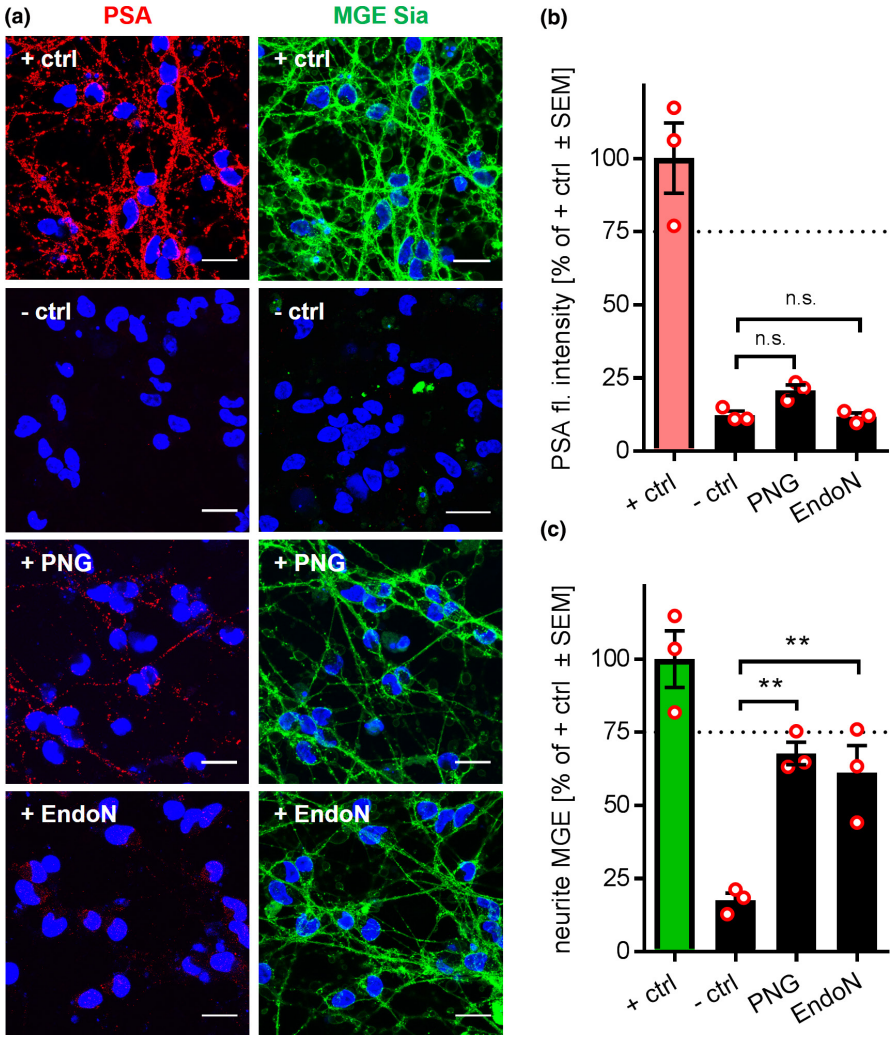

FIGURE 3 Detection of glycoengineered cell surface Sia in PSA and in other glycans. Mature LUHMES neurons, differentiated for 5 days, were treated with 10 μM Ac_4ManNAz and cell surface sialic acids (Sia) were stained 24 h later, after their coupling to biotin. After the live metabolic glycoengineering (MGE) staining, cells were fixed, and anti-polysialic acid (PSA) antibody, or no antibody, and H-33342 were used to further label polysialic acid-neural cell adhesion molecule (PSA-NCAM) and nuclei. The images in (a) show the same set of cells in each row (except of the second row, where individual controls for each staining were used). The top row shows representative images of typical stains and cultures (=positive control; +ctrl). The second row is a negative control (− ctrl) without PSA antibody and without MGE-biotin ligation, but with secondary antibody and labeled streptavidin added. For images in the third row, cells were treated with protein N-glycosidase F (+PNG) for 2 h before staining. For images in the fourth row, cells were treated with endoneuraminidase N (+ EndoN) for 2 h before staining. (a) Representative images of PSA immunostains (left) and cell surface sialic acids by MGE (right). Scale bar = 25 μm. (b) Quantification of PSA staining intensity. (c) Quantification of MGE Sia intensity. All data are presented as means from three independent biological replicates (=three independent cell preparations). Statistics: One-way ANOVA followed by Dunnett's test; $^{**}p < 0.01$ (all treatments vs.—ctrl), n.s., not significant.

in a 24 h co-treatment scheme (drug + Sia precursor sugar), in which viability, surface Sia MGE, and protein sialylation were assessed (Figure 4b). Both, dMM and NBdNM, neither affected the percentage of live cells nor the neurite area of mature LUHMES cells up to concentrations of 1 mM (Figure 4c). Western blot analysis of sialylated proteins showed a significant decrease (by 57%) in the MGE sialylated proteins when cells were treated with dMM and no effect of NBdNM. This confirmed their biochemical mode of action in our model system (Figure 4d). As second endpoint, fluorescence imaging of labeled Sia was used: NBdNM (which had shown no effect on protein sialylation) now caused a very strong response (60% attenuation of the signal). This showed that sialylated lipids (the target of NBdNM) contributed to a large degree to the neuronal Sia-MGE signal. In line with this, dMM treatment (reduction of N-linked sialoproteins) reduced the Sia-MGE signal by only 17%. The combination of both imino sugars virtually eliminated all Sia incorporation into plasma membranes. This effect was similar to the one observed after enzymatic removal of MGE Sia from the plasma membrane using sialidase (Figure 4e,f).

Besides quantification of the overall signal, we also studied qualitatively, whether the imino sugars altered the staining pattern of Sia-MGE: Selective stains of sialolipids on the plasma membrane (in the presence of dMM) appeared as dotted-like structures. This discontinuous pattern was confirmed by high resolution microscopy. It is unclear at present, why membranes stained this way. Possibly, it is related to membrane dynamics in the live cells or to sequestration of label in lipid rafts. The staining patter of sialoproteins (MGE signal in the presence of NBdNM) was faint, but always smooth, also when observed by high resolution microscopy. These findings provide independent evidence that different cellular structures are stained in the presence of the imino sugars dMM and NBdNM (Figure S3).

As specificity and consistency controls for our experimental system, we used two further glycosylation inhibitors. The Golgi mannosidase inhibitor swainsonine has a similar biochemical target as dMM. It decreased protein sialylation but had only minor effect (15%) on the Sia-MGE neuronal surfaces staining signal. These results were similar to those obtained for dMM, as expected from the claimed biochemical mechanism. As negative control, we used castanospermine, an imino sugar inhibiting ER glucosidase. As expected from its target specificity, this compound did not affect the MGE Sia levels (Figure S4).

As biochemical control of our immunostaining data, the absolute amounts of Sia in neuronal glycans were determined. In postmitotic LUHMES neurons, treatment with NBdNM (reduction of lipid sialoglycan content) reduced the overall amount of cellular Sia, while dMM (acting as sialoprotein inhibitor) had no significant effect. Data from this experiment are consistent with our previous findings that sialolipids contain an important fraction of overall cellular Sia. However, the signal–noise ratio of this approach was poor, as cells already had sialoglycans before the experiment (Figure S5a). Therefore, we also determined, how much the newly added Sia contributed to the overall Sia content. For this purpose, neurons were fed with an azide-tagged Sia precursor (SiaAz), and the percentage of tagged versus non-tagged Sia was measured as "incorporation efficiency." NBdNM significantly reduced incorporation (by preventing formation of new sialolipids), while dMM had no measureable effect (Figure S5b). These data clearly demonstrated the dominant role of lipid sialoglycans in the neuronal Sia content.

Finally, we asked whether similar effects were also observed for another neuronal model system. We found that also in peripheral neurons, dMM significantly decreased protein sialylation, while NBdNM had no effect on the sialoproteins (Figure 5a). Conversely,

FIGURE 4 Selective labeling of sialoproteins and sialolipids in LUHMES neurons by MGE. (a) Graphical representation of the principle strategy for specific labeling of sialolipids or sialoproteins: Deoxymannojirimycin (dMM) inhibits the incorporation of sialic acid (Sia) into glycoproteins. Its presence allows for the detection of metabolic glycoengineering (MGE)-labeled lipid Sia on the cellular plasma membrane. *N*-butyl deoxynojirimycin (NBdNM) inhibits the incorporation of Sia into glycolipids. Its presence allows for the detection of MGE-labeled Sia on proteins. (b) Scheme of experimental setup to test differential inhibition. LUHMES cells differentiated for 5 days (d5) were co-treated with *N*- azidoacetylmannosamine (Ac_4ManNAz; modified sugar) and either dMM or NBdNM for 24 h. Then, on day 6 (d6), cells were analyzed for viability (high content imaging), sialoproteins (Western blot of MGE labeled sialoproteins) and overall MGE Sia (confocal microscopy imaging). (c) Effects of imino sugars on neuronal viability. Cells were treated with dMM and NBdNM (10–1000 μM). Analysis was performed on live cells stained with H-33342/calcein-AM. Data are presented as means from three independent biological replicates (=three independent cell preparations). (d) Effects of dMM/NBdNM on neuronal MGE sialoprotein contents. After the exposure (24 h), cells were washed and MGE Sia on the surface of live cells was ligated to dibenzocyclooctyne (DBCO)-biotin (100 μM) for 20 min. Afterwards, cell lysates were prepared. Western blot against biotin was performed (anti-biotin antibody) to detect the labeled MGE sialylated proteins. Left: Representative membrane image. For orientation, the position of molecular weight markers (kDa) is indicated on the left hand side. Right: Quantification of MGE sialoproteins by densitometric analysis of the blots. Data are presented as means from three independent biological replicates (=three independent cell preparations); statistics: One-way ANOVA followed by Dunnett's test; n.s. = not significant, $^{***}p < 0.001$ (inhibitors vs. solvent control). (e) MGE labeling of sialolipids or sialoproteins. Representative images for six staining conditions are shown. The top row shows representative images of all Sia proteins and lipids (ManNAz-treated and MGE labeled cells; +ctrl) and negative controls (without the modified sugar and without labeled Sia; −ctrl). The second row shows Sia lipids (without Sia proteins; +dMM), and Sia proteins (without Sia lipids; +NBdNM). For images in the third row, all cell surface sialylated glycans were blocked (co-treatment with dMM and NBdNM) or all Sia glycans were removed (enzymatic treatment with sialidase V (siaV) for 2 h before MGE and fixation). Scale bar = 25 μm. (f) Quantification of MGE. Data are means from three independent biological replicates (=three independent cell preparations) and are presented as percentage of Ac_4ManNAz-treated control (+ctrl). Statistics I (against − Ctrl): One-way ANOVA followed by Dunnett's test; n.s. = not significant, $^{*}p < 0.05$, $^{***}p < 0.001$ (inhibitors and enzyme vs. solvent control [−ctrl]). Statistics II (not shown, against + ctrl): siaV, NBdNM, dMM + NBdNM were significantly reduced, dMM was n.s.

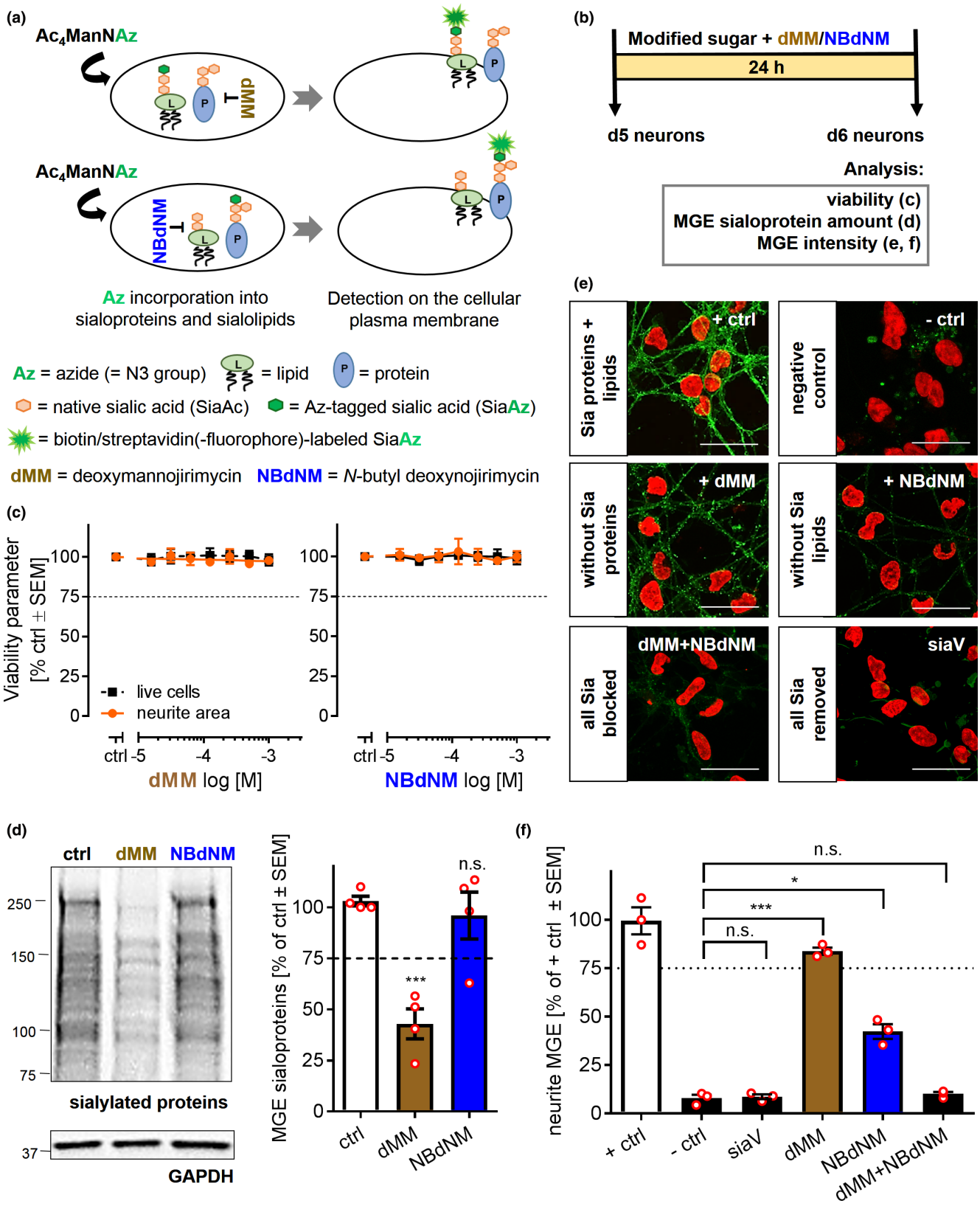

NBdNM inhibition of lipid sialylation led to an almost complete removal of MGE Sia signals detected by immunostaining on neurites, while some significant stain was left in the presence of dMM. The combination of dMM and NBdNM completely removed the neurite MGE signal (Figure 5b,c).

The data from this set of experiments suggest that MGE labels sialoproteins and sialolipids on neurons. Sialylated lipids contributed quantitatively to a higher degree to the MGE Sia stain than the glycoproteins. The novel strategy using glycosidase inhibitors during the MGE procedure allows for separate studies of sialolipids (after

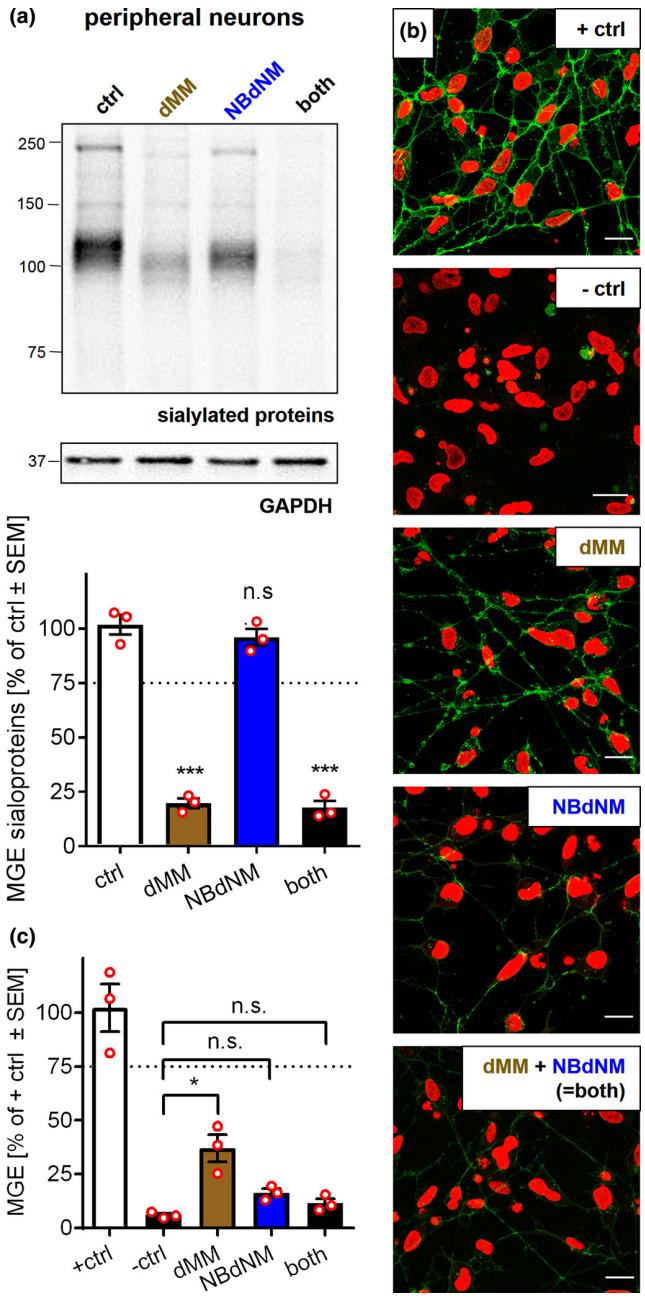

FIGURE 5 Selective MGE sialoprotein and sialolipid detection in peripheral neurons. Peripheral neurons, differentiated for 4 days, were co-treated with *N*-azidoacetylmannosamine (Ac_4ManNAz) and deoxymannojirimycin (dMM, 1 mM), *N*-butyl deoxynojirimycin (NBdNM, 1 mM), or a combination of both. After 24 h, metabolic glycoengineering (MGE) sialylated proteins (Western blot) and neuronal MGE (confocal microscopy) were analyzed. (a) Top: Representative membrane image of MGE sialoproteins levels. For orientation, the position of molecular weight markers (kDa) is indicated on the left hand side. Bottom: Quantification of MGE sialoproteins. Data are presented as means from three independent biological replicates (=three independent cell preparations). Statistics: One-way ANOVA followed by Dunnett's test; n.s. = not significant, $^{***}p < 0.001$ (inhibitors vs. solvent control). (b) Selective labeling of sialolipids or sialoproteins by MGE. Staining was performed as in Figure 4. Representative confocal images show MGE sialoglycans (green) and nuclei (red). (c) Quantification of cell surface MGE. Both = dMM + NBdNM co-treated. All data are means from three independent biological replicates (=three independent cell preparations) and are presented as percentage of Ac_4ManNAz-treated control (+ ctrl). Statistics: One-way ANOVA followed by Dunnett's test; n.s. = not significant, $^{*}p < 0.05$ (inhibitors vs. Ac_4ManNAz-untreated control [− ctrl]).

dMM treatment) or sialoproteins (after NBdNM treatment) on live cells.

3.5 | Temporal resolution of lipid and protein glycoinhibition

For the use of the inhibitor-combined MGE approach to visualize, for example, sialolipids in various experimental situations, it would be desirable to obtain data with a higher time resolution. We knew from extensive earlier characterizations that it takes around 6 h from the point neurons are fed the Sia precursor, until they display it on the neuronal surface as labeled Sia (Kranaster et al., 2020). We wondered whether the specific glycosidase inhibition was already observable within such a time frame: Mature LUHMES were treated with the azide Sia precursor for 6 h. The imino sugars were given during the same time, or 18 h earlier (positive control of effect) or 2 h later (minimizing the time resolution window, accounting for a time that the externally added sugars need to penetrate into the cells and enter the biosynthetic pathways). Finally, the inhibitors were added only during the last hour of incubation. We assumed that this should at best have a minor effect as the inhibitor was only present during a small (≤20%–25%) fraction of the time that the cells had to synthesize and translocate the Sia glycans to the membrane (Figure 6a). We observed that a significant effect of dMM on protein MGE Sia required only 4 h of treatment, and a maximal effect was obtained at 4–6 h (NBdNM had no effect at all, as expected) (Figure 6b, Figure S6). As gangliosides and PSA-NCAM play particularly important roles in the growing neurites, we next used an algorithm to identify neurites and to measure MGE signals after glycoinhibition only on these structures. This way, we obtained a neurite area-normalized MGE intensity (called here neurite MGE). When the neurite MGE was examined, dMM caused a drop by 25% within 4 h. This minor inhibition did not increase with longer treatment times. With NBdNM, even a short treatment of 1 h already significantly reduced the neurite MGE signal (by 25%), and maximal inhibitions of about 60% were reached after 4–6 h. None of the treatments affected the viability of cells or the overall neurite area (Figure 6c, Figure S7).

These results show that time resolutions of few hours can be reached, when dynamic changes in cells are examined (e.g., in disease models or upon drug treatment). The data from these experiments also indicate a surprisingly high turnover of membrane components in cultured neurons. They suggest an exchange of at least 25% of sialolipids and sialoproteins within few hours. It is unclear whether this occurs by processing of only the carbohydrate part, or by degradation and re-synthesis of the entire glycoproteins and gangliosides.

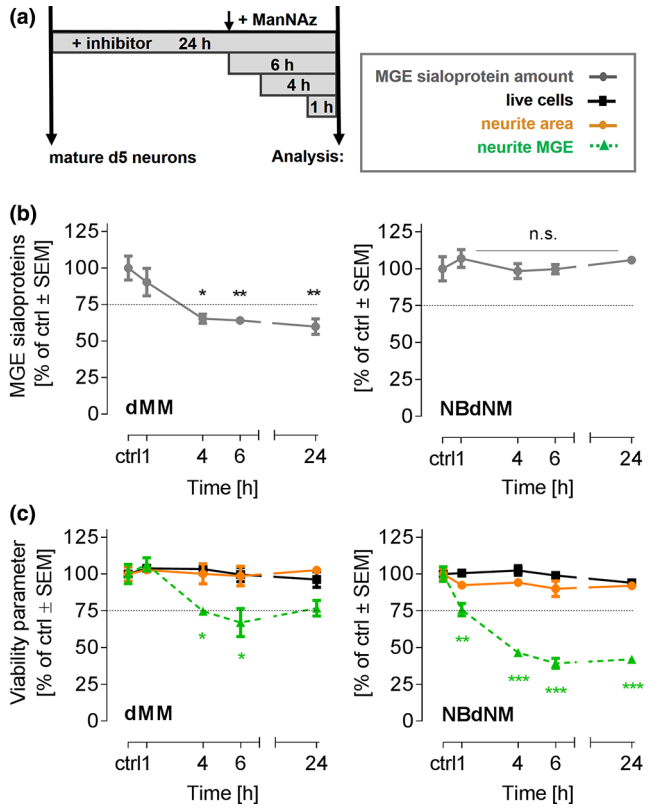

FIGURE 6 Temporal resolution of the analysis of sialoproteins and sialolipids by selective MGE inhibition. (a) Scheme of the experimental setup. LUHMES cells were differentiated for 5 days (d5) and treated with inhibitors for a duration of 1, 4, 6, and 24 h. *N*-azidoacetylmannosamine (Ac_4ManNAz) (+ManNAz, 10 μM) was added for the last 6 h. note, that the need for this labeling time has been determined earlier (Kranaster et al., 2020) and that some time is needed for the modified sugar to enter the cell and the biosynthetic pathways. After the end of the experiment, cells were washed and ligated to dibenzocyclooctyne (DBCO)-biotin. Afterwards, cells were either lysed for Western blotting or stained with a mixture of H-33342, CellTrace™ Calcein red–Orange and fluorescent streptavidin (strep-AF488) and analyzed by confocal microscopy. (b) Time–response curves of metabolic glycoengineering (MGE) sialoglycoprotein inhibition (by Western blot quantification) after deoxymannojirimycin (dMM, 1 mM) or *N*-butyl deoxynojirimycin (NBdNM, 1 mM) treatment. Data are presented as means from three independent biological replicates (=three independent cell preparations). (c) Changes of viability (solid black line), neurite area (solid orange line), and neurite MGE (dashed green line) after dMM or NBdNM inhibition. All data are means from three independent biological replicates (=three independent cell preparations). Statistics: One-way ANOVA followed by Dunnett's test; $^{*}p<0.05$, $^{**}p<0.01$, $^{***}p<0.001$ (treated time points vs. solvent control).

3.6 | Extension of sialolipid versus sialoprotein profiling to diverse cell types

The labeling technique developed here is likely to be applicable to other cell types. To explore this, we investigated in a small case study, whether the high ratio of sialolipids versus sialoproteins is also found in non-neuronal cells. We chose HepG2 hepatoma cells as additional cell type, as they differ from neurons concerning biological features, origins, and functions. MGE labeling of their membranes worked just as in neurons, and the imino sugars were well-tolerated. Treatment with dMM strongly (>70%) decreased the amount of labeled sialoproteins (Western blot analysis), whereas NBdNM had no effect on this endpoint (Figure 7a). These findings were essentially similar as in neurons, but the dMM effect was more pronounced.

Next, quantitative imaging of the membrane MGE signal was performed: here, dMM reduced the signal strongly, whereas no significant change occurred under treatment with NBdNM (Figure 7b,c). These effects are largely different from those observed in neurons. They point to a low sialolipid content and a high sialoprotein fraction in HepG2 cells, and this is fully in line with literature data that measured the ratio of sialoglycans in liver and brain (Schnaar et al., 2014).

As a third exemplary cell type, we examined neural crest cells. These fetal cells give rise to, for example, melanocytes, craniofacial bone, and cartilage, as well as peripheral neurons (Achilleos & Trainor, 2012). As expected, dMM inhibited the incorporation of Sia into glycoproteins, while NBdNM had no effect on protein sialylation (Figure 8a). When the membrane MGE signal was quantified, it became clear that dMM had a pronounced inhibitory effect (>60%), while there was only a minor effect of NBdNM treatment. Cells treated with dMM plus NBdNM had an MGE signal that did not differ from negative controls (Figure 8b,c). Thus, neural crest cells had a membrane sialoglycan distribution (protein vs. lipid), similar to HepG2 cells and different from neurons.

This application example showed that different cell types can have largely different ratios of sialoglycan types, exemplified here by two neuronal cultures with a dominance of sialolipids, versus HepG2 and neural crest cells with a dominance of sialoproteins.

4 | DISCUSSION AND CONCLUSIONS

We confirmed here for several human culture systems that sialoglycoconjugates can be visualized on the membranes of live neurons, based on simple feeding of the neurons with azide-tagged mannosamine. Two case studies, using differentiating neurons with low levels of membrane NCAM and post-mitotic neurons with abundant PSA-NCAM, showed that a large proportion of neuronal sialoglycoconjugates are not restricted to polysialylated forms of NCAM. Triggered by this observation, we reasoned that sialolipids may play a hitherto underestimated role. To investigate this question, we developed here a novel approach to combine MGE with inhibition of certain glycosylation pathways. The use of dMM allowed a selective visualization of sialoglycolipids on membranes of neurons and other cells, while the use of NBdNM allowed the preferential visualization of protein-linked Sia. Application of this novel method showed that different cell types have largely different proportions of sialoproteins and sialolipids. This technical approach will allow more specific future observations of sialoglycans on live cells. While the fluorescently labeled molecules can be

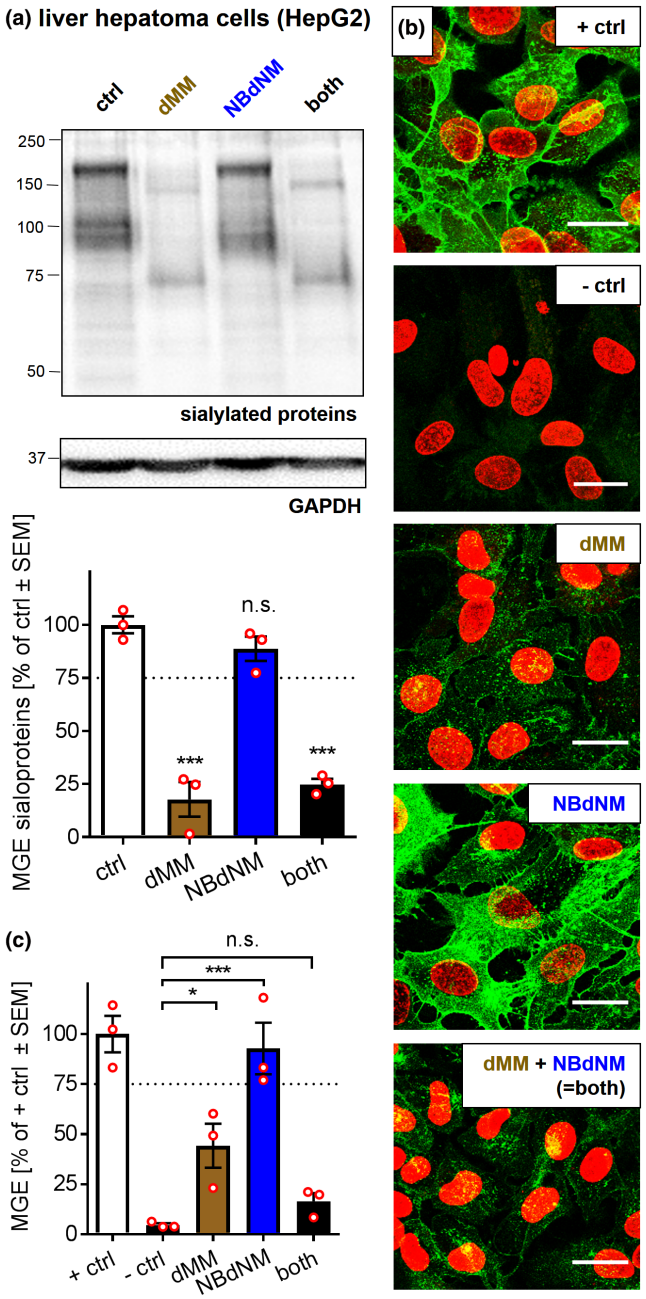

FIGURE 7 Selective MGE sialoprotein and sialolipid detection in liver hepatoma cells. HepG2 cells were co-treated with *N*-azidoacetylmannosamine (Ac_4ManNAz) and deoxymannojirimycin (dMM, 1 mM), *N*-butyl deoxynojirimycin (NBdNM, 1 mM), or a combination of both. After 24 h, metabolic glycoengineering (MGE) sialoproteins (Western blot) and surface MGE (confocal microscopy) were analyzed. (a) Top: Representative membrane image of MGE sialoproteins levels. For orientation, the position of molecular weight markers (kDa) is indicated on the left hand side. Bottom: Quantification of MGE sialoproteins. Data are presented as means from three independent biological replicates (= three independent cell preparations). Statistics: One-way ANOVA followed by Dunnett's test; n.s. = not significant, $^{***}p < 0.001$ (inhibitors vs. solvent control). (b) Selective labeling of sialolipids or sialoproteins by MGE. Staining was performed as in Figure 4. Representative confocal images show MGE sialoglycans (green) and nuclei (red). (c) Quantification of surface MGE. Both = dMM + NBdNM co-treated. All data are means from three independent biological replicates (=three independent cell preparations) and are presented as percentage of Ac_4ManNAz-treated control (+ ctrl). Statistics: One-way ANOVA followed by Dunnett's test; n.s. = not significant, $^{*}p < 0.05$, $^{***}p < 0.001$ (inhibitors vs. Ac_4ManNAz-untreated control [− ctrl]).

followed in real time (similar to e.g., GFP-tagged proteins), the incorporation of new metabolic precursors can be observed within a time resolution of few hours. This is somewhat slower than for de novo expression of fluorescent proteins, but still within the same order of magnitude.

4.1 | Use of glycosidase inhibitors

The separate observation of protein versus lipid Sia was achieved here by glycosidase inhibition. It may not be entirely clear to non-specialists, why glycosidase inhibitors prevent the addition of Sia to glycoproteins. The background is that the synthesis of N-glycosylated proteins is a complex process that involves an intermediate, but essential trimming step. Initially, a preformed mannose-rich structure ($Glc_3Man_9GlcNAc_2$, a 14-meric sugar containing nine mannoses and three glucoses) is transferred to an asparagine of the protein. Then mannose residues need to be trimmed in the Golgi to allow the synthesis of the mature glycan with Sia as terminal sugars. If the enzymes removing mannose are blocked, the whole process is stalled. Notably, also some glucosidases are involved in the trimming process. The removal of two glucose moieties is essential for ER quality control. However, there is a large variety of glucosidases, and the alpha-glucosidase inhibitors castanospermine (Figure S4) or deoxynojirimycin (data not shown) did not affect sialylation, as they target other cellular processes. The most efficient inhibition of the protein sialylation was observed after inhibition of alpha-mannosidase with dMM and Swa. These compounds inhibit the Golgi alpha-mannosidase II and I, respectively: they cause the accumulation of hybrid-type (partially processed) carbohydrate chains at the cost of mature (complex) oligosaccharides. As Sia is found mostly at the ends of the complex-type oligosaccharide chains, inhibition of these type of glycans resulted in a decreased MGE signal in our model system.

It needs to be mentioned here, that N-linked protein glycosylation is not the only modification of proteins with carbohydrates. Another, biologically very important, process is the O-linked β-*N*-acetylglucosamine (O-GlcNAc) modification of proteins (Hart & Akimoto, 2009). This process is involving only a single carbohydrate, often has intracellular targets, and does not involve Sia. Finally, some complex carbohydrates can be added to serine or threonine residues of proteins as O-linked glycans. Such structures take important biological roles as mucins, proteoglycans or in the immune system. However, their contribution to the neuronal sialoglycan content is usually low and was therefore not considered here.

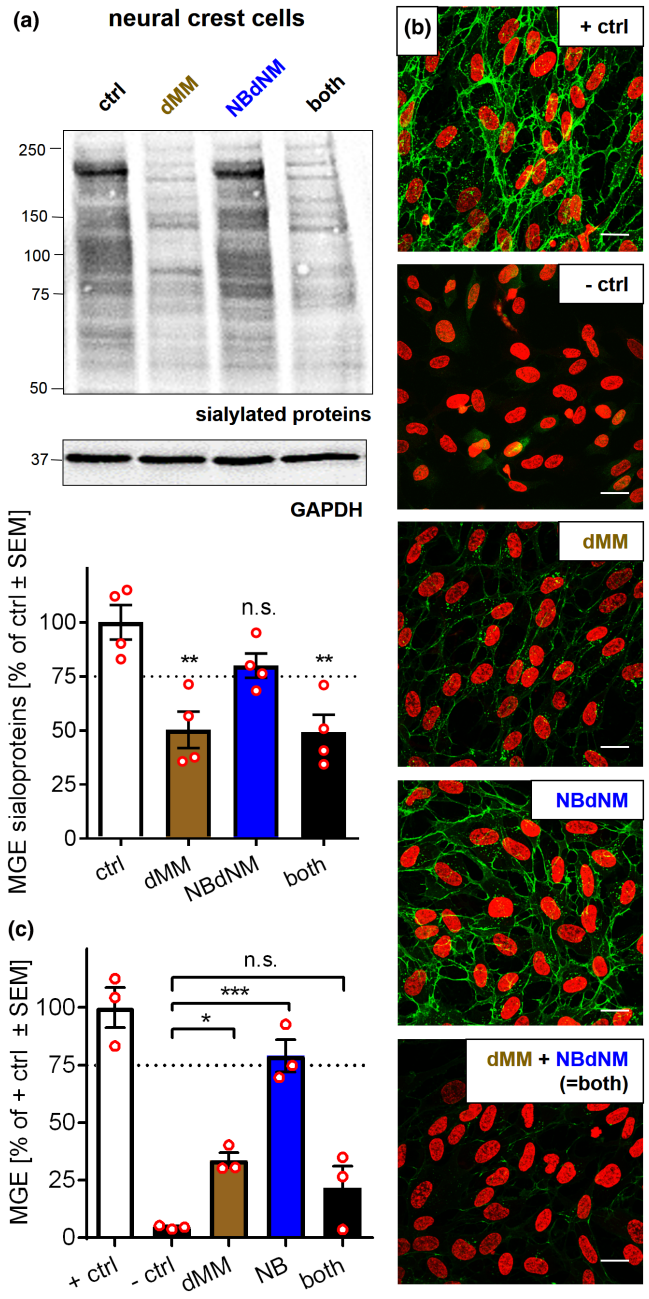

FIGURE 8 Selective MGE sialoprotein and sialolipid detection in neural crest cells. Neural crest cells were co-treated with *N*-azidoacetylmannosamine (Ac_4ManNAz) and deoxymannojirimycin (dMM, 1 mM), *N*-butyl deoxynojirimycin (NBdNM, 1 mM), or a combination of both. After 24 h, metabolic glycoengineering (MGE) sialoproteins (Western blot) and surface MGE (confocal microscopy) were analyzed. (a) Top: Representative membrane image of MGE sialoproteins levels. For orientation, the position of molecular weight markers (kDa) is indicated on the left hand side. Bottom: Quantification of MGE sialoproteins. All data are presented as means from three independent biological replicates (=three independent cell preparations). Statistics: One-way ANOVA followed by Dunnett's test; n.s. = not significant, $^{**}p < 0.01$ (inhibitors vs. solvent control). (b) Selective labeling of sialolipids or sialoproteins by MGE. Staining was performed as in Figure 4. Representative confocal images show MGE sialoglycans (green) and nuclei (red). (c) Quantification of surface MGE. Both = dMM + NBdNM co-treated. All data are means from three independent biological replicates (=three independent cell preparations) and are presented as percentage of Ac_4ManNAz-treated control (+ ctrl). Statistics: One-way ANOVA followed by Dunnett's test; n.s. = not significant, $^{*}p < 0.05$, $^{***}p < 0.001$ (inhibitors vs. Ac_4ManNAz-untreated control [− ctrl]).

4.2 | Ganglioside labeling

Gangliosides (glycosylated sphingolipids) have a wide variety of biological functions. They form a critical component of membrane rafts, or ganglioside-enriched microdomains, where they influence the physical properties of the membrane as well as its function (Sipione et al., 2020). They can change their structure to meet their external and internal environmental demands (Wang & Whitehead, 2020). This means biochemically, that sugar units (including Sia) can be added or removed. Ganglioside dysregulation is observed in several lysosomal storage disorders diseases, including Tay Sach's disease (Platt et al., 2018). The imino sugars used here have been developed in the context of research focused on providing help to patients with such diseases (Picache et al., 2022). Altered ganglioside patterns are also found in the aging brain as well as in several neurodegenerative injuries and diseases such as stroke, Alzheimer's disease, Parkinson's disease, and Huntington's disease (Ariga et al., 2008; Sipione et al., 2020; Yamashita et al., 2005). The method developed here adds to the toolbox of methods required to better understand metabolism and distribution of sialyl-gangliosides.

4.3 | Outlook

While visualization and analysis of proteins and nucleic acids have become standard techniques, approaches to localize glycans are still only used by some specialized laboratories. MGE has become an important technique, in addition to, for example, the use of antibodies and lectins. The large variety of carbohydrate structures (thousands), and of processing enzymes (>100) still poses a great challenge. Our method allows now at least the separate visualization of two major groups of sialylated glycans. The data still need to be interpreted carefully, and solid conclusions will require extensive characterizations of the respective experimental model and running of several controls. However, we believe that further developments are possible, for example, by using of additional inhibitors and the combination of various MGE substrates. It is for instance possible to use two tags that may be labeled by different fluorescent molecules (Schart et al., 2019). A further advance would be to target various cell compartments and organelles. Here we used live cells as they allowed for an unmatched signal–noise ratio. The technique is also applicable to intracellular compartments, but then optimized fixation techniques are required. Various FRET and BRET approaches can provide information on the local environment of glycans (Doll et al., 2018). In the context of neurons, it would be interesting to optimize the method toward a specific recognition of PSA. Possibly the

sequential or mixed use of Sia precursors that can be labeled by different fluorescent molecules could be used to define polysialylated structures through the quantification of FRET or fluorescence quenching effects. Such approaches have been considered earlier, but the possibility to avoid the labeling of lipids (in the presence of e.g., NBdNM), would largely facilitate such approaches.

AUTHOR CONTRIBUTIONS

P.K. designed and performed most of the experiments, analyzed and interpreted the data, and wrote the manuscript; J.B. performed pilot experiments for the study and proofread the manuscript; J.D. designed and performed the experiments, analyzed the data and proofread the manuscript; V.W. designed the experiments, proofread the manuscript, and obtained funding; M.L. designed the experiments, wrote the manuscript and obtained funding.

ACKNOWLEDGMENTS

This work was supported by the Doerenkamp-Zbinden foundation, the Deutsche Forschungsgemeinschaft (KoRS-CB; SFB 969–project B05), the European Food Safety Authority, the State Ministry of Baden-Wuerttemberg Germany for Economic Affairs, Labour and Tourism (NAM-Accept), and the BMBF (NeuroTool). It has also received funding from the European Union's Horizon 2020 research and innovation program under grant agreements No. 964537 (RISK-HUNT3R), and no. 964518 (ToxFree). The Bioimaging Center of the University of Konstanz is acknowledged for providing an outstanding support and the confocal and OMX microscopy instrumentation. We thank Mariannne Wiechers for her excellent technical assistance with Western blot experiments, Dr. Lisa Hölting, Dr. Stefanie Klima, and Dr. Anna-Katharina Holzer for differentiation, freezing, and seeding of the peripheral neurons, as well as Dr. Johanna Nyffeler and Dr. Xenia Dolde for differentiation, freezing, and seeding of the neural crest cells. Christiaan Karreman is acknowledged for the development of the ImaEva and SUIKER programs. Open Access funding enabled and organized by Projekt DEAL.

CONFLICT OF INTEREST

M. Leist is an Editor for the Journal of Neurochemistry. The other authors declare no conflict of interest.

DATA AVAILABILITY STATEMENT

The data that support the findings of this study are available from the corresponding author upon reasonable request.

ORCID

Petra Kranaster https://orcid.org/0000-0002-6082-0161
Valentin Wittmann https://orcid.org/0000-0003-4043-6813
Marcel Leist https://orcid.org/0000-0002-3778-8693

REFERENCES

Achilleos, A., & Trainor, P. A. (2012). Neural crest stem cells: Discovery, properties and potential for therapy. *Cell Research*, *22*(2), 288–304. https://doi.org/10.1038/cr.2012.11

Aonurm-Helm, A., Jaako, K., Jurgenson, M., & Zharkovsky, A. (2016). Pharmacological approach for targeting dysfunctional brain plasticity: Focus on neural cell adhesion molecule (NCAM). *Pharmacological Research*, *113*(Pt B), 731–738. https://doi.org/10.1016/j.phrs.2016.04.011

Ariga, T., McDonald, M. P., & Yu, R. K. (2008). Role of ganglioside metabolism in the pathogenesis of Alzheimer's disease—A review. *Journal of Lipid Research*, *49*(6), 1157–1175. https://doi.org/10.1194/jlr.R800007-JLR200

Bonfanti, L. (2006). PSA-NCAM in mammalian structural plasticity and neurogenesis. *Progress in Neurobiology*, *80*(3), 129–164. https://doi.org/10.1016/j.pneurobio.2006.08.003

Butters, T. D., Dwek, R. A., & Platt, F. M. (2000). Inhibition of glycosphingolipid biosynthesis: Application to lysosomal storage disorders. *Chemical Reviews*, *100*(12), 4683–4696.

Butters, T. D., Dwek, R. A., & Platt, F. M. (2005). Imino sugar inhibitors for treating the lysosomal glycosphingolipidoses. *Glycobiology*, *15*(10), 43R–52R. https://doi.org/10.1093/glycob/cwi076

Campbell, C. T., Sampathkumar, S. G., & Yarema, K. J. (2007). Metabolic oligosaccharide engineering: Perspectives, applications, and future directions. *Molecular BioSystems*, *3*(3), 187–194. https://doi.org/10.1039/b614939c

Chen, G., Gulbranson, D. R., Hou, Z., Bolin, J. M., Ruotti, V., Probasco, M. D., Smuga-Otto, K., Howden, S. E., Diol, N. R., Propson, N. E., Wagner, R., Lee, G. O., Antosiewicz-Bourget, J., Teng, J. M. C., & Thomson, J. A. (2011). Chemically defined conditions for human iPSC derivation and culture. *Nature Methods*, *8*(5), 424–429. https://doi.org/10.1038/nmeth.1593

Chovancova, P., Merk, V., Marx, A., Leist, M., & Kranaster, R. (2017). Reverse-transcription quantitative PCR directly from cells without RNA extraction and without isothermal reverse-transcription: A 'zero-step' RT-qPCR protocol. *Biology Methods & Protocols*, *2*(1), bpx008. https://doi.org/10.1093/biomethods/bpx008

Delp, J., Funke, M., Rudolf, F., Cediel, A., Bennekou, S. H., van der Stel, W., Carta, G., Jennings, P., Toma, C., Gardner, I., van de Water, B., Forsby, A., & Leist, M. (2019). Development of a neurotoxicity assay that is tuned to detect mitochondrial toxicants. *Archives of Toxicology*, *93*(6), 1585–1608. https://doi.org/10.1007/s00204-019-02473-y

Dold, J., Pfotzer, J., Spate, A. K., & Wittmann, V. (2017). Dienophile-modified Mannosamine derivatives for metabolic labeling of sialic acids: A comparative study. *Chembiochem*, *18*(13), 1242–1250. https://doi.org/10.1002/cbic.201700002

Dold, J., & Wittmann, V. (2021). Metabolic Glycoengineering with Azide- and alkene-modified Hexosamines: Quantification of sialic acid levels. *Chembiochem*, *22*(7), 1243–1251. https://doi.org/10.1002/cbic.202000715

Dolde, X., Karreman, C., Wiechers, M., Schildknecht, S., & Leist, M. (2021). Profiling of human neural crest chemoattractant activity as a replacement of fetal bovine serum for In vitro chemotaxis assays. *International Journal of Molecular Sciences*, *22*(18). https://doi.org/10.3390/ijms221810079

Doll, F., Hassenruck, J., Wittmann, V., & Zumbusch, A. (2018). Intracellular imaging of protein-specific glycosylation. *Methods in Enzymology*, *598*, 283–319. https://doi.org/10.1016/bs.mie.2017.06.015

Dube, D. H., & Bertozzi, C. R. (2003). Metabolic oligosaccharide engineering as a tool for glycobiology. *Current Opinion in Chemical Biology*, *7*(5), 616–625. https://doi.org/10.1016/j.cbpa.2003.08.006

Finne, J., Finne, U., Deagostini-Bazin, H., & Goridis, C. (1983). Occurrence of alpha 2-8 linked polysialosyl units in a neural cell adhesion molecule. *Biochemical and Biophysical Research Communications*, *112*(2), 482–487. https://doi.org/10.1016/0006-291x(83)91490-0

Fleet GW, Fellows LE, Winchester B (1990) Plagiarizing plants: Amino sugars as a class of glycosidase inhibitors. *Ciba Foundation Symposium 154*:112–22; discussion 122–5.

Goodfellow, J. A., & Willison, H. J. (2016). Antiganglioside, antiganglioside-complex, and antiglycolipid-complex antibodies in immune-mediated neuropathies. *Current Opinion in Neurology*, *29*(5), 572–580. https://doi.org/10.1097/WCO.0000000000000361

Goridis, C., & Brunet, J. F. (1992). NCAM: Structural diversity, function and regulation of expression. *Seminars in Cell Biology*, *3*(3), 189–197. https://doi.org/10.1016/s1043-4682(10)80015-7

Gruters, R. A., Neefjes, J. J., Tersmette, M., de Goede, R. E. Y., Tulp, A., Huisman, H. G., Miedema, F., & Ploegh, H. L. (1987). Interference with HIV-induced syncytium formation and viral infectivity by inhibitors of trimming glucosidase. *Nature*, *330*(6143), 74–77. https://doi.org/10.1038/330074a0

Gutbier, S., May, P., Berthelot, S., Krishna, A., Trefzer, T., Behbehani, M., Efremova, L., Delp, J., Gstraunthaler, G., Waldmann, T., & Leist, M. (2018). Major changes of cell function and toxicant sensitivity in cultured cells undergoing mild, quasi-natural genetic drift. *Archives of Toxicology*, *92*(12), 3487–3503. https://doi.org/10.1007/s00204-018-2326-5

Gutbier, S., Spreng, A. S., Delp, J., Schildknecht, S., Karreman, C., Suciu, I., Brunner, T., Groettrup, M., & Leist, M. (2018). Prevention of neuronal apoptosis by astrocytes through thiol-mediated stress response modulation and accelerated recovery from proteotoxic stress. *Cell Death and Differentiation*, *25*(12), 2101–2117. https://doi.org/10.1038/s41418-018-0229-x

Hart, G. W., & Akimoto, Y. (2009). Chapter 18, The O-GlcNAc modification. In A. Varki, R. D. Cummings, J. D. Esko, H. H. Freeze, P. Stanley, C. R. Bertozzi, G. W. Hart, and M. E. Etzler (Eds.), *Essentials of Glycobiology* (2nd ed.). Cold Spring Harbor Laboratory Press.

Hayes, J. M., O'Hara, D. M., & Davey, G. P. (2022). Metabolic labeling of primary neurons using carbohydrate click chemistry. *Methods in Molecular Biology*, *2370*, 315–322. https://doi.org/10.1007/978-1-0716-1685-7_16

Hoffman, S., Sorkin, B. C., White, P. C., Brackenbury, R., Mailhammer, R., Rutishauser, U., Cunningham, B. A., & Edelman, G. M. (1982). Chemical characterization of a neural cell adhesion molecule purified from embryonic brain membranes. *The Journal of Biological Chemistry*, *257*(13), 7720–7729.

Holzer, A. K., Suciu, I., Karreman, C., Goj, T., & Leist, M. (2022). Specific attenuation of purinergic signaling during Bortezomib-induced peripheral neuropathy In vitro. *International Journal of Molecular Sciences*, *23*(7). https://doi.org/10.3390/ijms23073734

Jackson, S. N., Ugarov, M., Egan, T., Post, J. D., Langlais, D., Albert Schultz, J., & Woods, A. S. (2007). MALDI-ion mobility-TOFMS imaging of lipids in rat brain tissue. *Journal of Mass Spectrometry*, *42*(8), 1093–1098. https://doi.org/10.1002/jms.1245

Kaczmarek, B., Verbavatz, J. M., & Jackson, C. L. (2017). GBF1 and Arf1 function in vesicular trafficking, lipid homoeostasis and organelle dynamics. *Biology of the Cell*, *109*(12), 391–399. https://doi.org/10.1111/boc.201700042

Kang, K., Joo, S., Choi, J. Y., Geum, S., Hong, S. P., Lee, S. Y., Kim, Y. H., Kim, S. M., Yoon, M. H., Nam, Y., Lee, K. B., Lee, H. Y., & Choi, I. S. (2015). Tissue-based metabolic labeling of polysialic acids in living primary hippocampal neurons. *Proceedings of the National Academy of Sciences of the United States of America*, *112*(3), E241–E248. https://doi.org/10.1073/pnas.1419683112

Karreman, C., Kranaster, P., & Leist, M. (2019). SUIKER: Quantification of antigens in cell organelles, neurites and cellular sub-structures by imaging. *ALTEX*, *36*(3), 518–520. https://doi.org/10.14573/altex.1906251

Kiselyov, V. V., Soroka, V., Berezin, V., & Bock, E. (2005). Structural biology of NCAM homophilic binding and activation of FGFR. *Journal of Neurochemistry*, *94*(5), 1169–1179. https://doi.org/10.1111/j.1471-4159.2005.03284.x

Ko, K. R., Tam, N. W., Teixeira, A. G., & Frampton, J. P. (2020). SH-SY5Y and LUHMES cells display differential sensitivity to MPP+, tunicamycin, and epoxomicin in 2D and 3D cell culture. *Biotechnology Progress*, *36*(2), e2942. https://doi.org/10.1002/btpr.2942

Kranaster, P., Karreman, C., Dold, J., Krebs, A., Funke, M., Holzer, A. K., Klima, S., Nyffeler, J., Helfrich, S., Wittmann, V., & Leist, M. (2020). Time and space-resolved quantification of plasma membrane sialylation for measurements of cell function and neurotoxicity. *Archives of Toxicology*, *94*(2), 449–467. https://doi.org/10.1007/s00204-019-02642-z

Maccioni, H. J., Quiroga, R., & Spessott, W. (2011). Organization of the synthesis of glycolipid oligosaccharides in the Golgi complex. *FEBS Letters*, *585*(11), 1691–1698. https://doi.org/10.1016/j.febslet.2011.03.030

Maley, F., Trimble, R. B., Tarentino, A. L., & Plummer, T. H., Jr. (1989). Characterization of glycoproteins and their associated oligosaccharides through the use of endoglycosidases. *Analytical Biochemistry*, *180*(2), 195–204. https://doi.org/10.1016/0003-2697(89)90115-2

MBS, L. (2019). Diagnostic histochemistry in neuropathology. *Seminars in Diagnostic Pathology*, *36*(1), 71–82. https://doi.org/10.1053/j.semdp.2018.10.004

Muhlenhoff, M., Eckhardt, M., & Gerardy-Schahn, R. (1998). Polysialic acid: Three-dimensional structure, biosynthesis and function. *Current Opinion in Structural Biology*, *8*(5), 558–564. https://doi.org/10.1016/s0959-440x(98)80144-9

Picache, J. A., Zheng, W., & Chen, C. Z. (2022). Therapeutic strategies for Tay-Sachs disease. *Frontiers in Pharmacology*, *13*, 906647. https://doi.org/10.3389/fphar.2022.906647

Platt, F. M., & Butters, T. D. (1998). New therapeutic prospects for the glycosphingolipid lysosomal storage diseases. *Biochemical Pharmacology*, *56*(4), 421–430.

Platt, F. M., d'Azzo, A., Davidson, B. L., Neufeld, E. F., & Tifft, C. J. (2018). Lysosomal storage diseases. *Nature Reviews. Disease Primers*, *4*(1), 27. https://doi.org/10.1038/s41572-018-0025-4

Platt, F. M., Neises, G. R., Dwek, R. A., & Butters, T. D. (1994). N-butyldeoxynojirimycin is a novel inhibitor of glycolipid biosynthesis. *The Journal of Biological Chemistry*, *269*(11), 8362–8365.

Porter, M. J., Zhang, G. L., & Schnaar, R. L. (2021). Ganglioside extraction, purification and profiling. *Journal of Visualized Experiments*, *169*. https://doi.org/10.3791/62385

Rudd, P., Karlsson, N. G., Khoo, K. H., & Packer, N. H. (2022). Chapter 51, Glycomics and glycoproteomics. In A. Varki, R. D. Cummings, J. D. Esko, P. Stanley, G. W. Hart, M. Aebi, D. Mohnen, T. Kinoshita, N. H. Packer, J. H. Prestegard, R. L. Schnaar, & P. H. Seeberger (Eds.), *Essentials of Glycobiology* (4th ed., pp. 653–666). Cold Spring Harbor Laboratory Press.

Rueden, C. T., Schindelin, J., Hiner, M. C., DeZonia, B., Walter, A. E., Arena, E. T., & Eliceiri, K. W. (2017). ImageJ2: ImageJ for the next generation of scientific image data. *BMC Bioinformatics*, *18*(1), 529. https://doi.org/10.1186/s12859-017-1934-z

Sarbu, M., Fabris, D., Vukelic, Z., Clemmer, D. E., & Zamfir, A. D. (2022). Ion mobility mass spectrometry reveals rare Sialylated glycosphingolipid structures in human cerebrospinal fluid. *Molecules*, *27*(3). https://doi.org/10.3390/molecules27030743

Saxon, E., & Bertozzi, C. R. (2000). Cell surface engineering by a modified Staudinger reaction. *Science*, *287*(5460), 2007–2010. https://doi.org/10.1126/science.287.5460.2007

Saxon, E., Luchansky, S. J., Hang, H. C., Yu, C., Lee, S. C., & Bertozzi, C. R. (2002). Investigating cellular metabolism of synthetic azidosugars with the Staudinger ligation. *Journal of the American Chemical Society*, *124*(50), 14893–14902. https://doi.org/10.1021/ja027748x

Schart, V. F., Hassenruck, J., Spate, A. K., Dold, J., Fahrner, R., & Wittmann, V. (2019). Triple orthogonal labeling of Glycans by applying Photoclick chemistry. *Chembiochem*, *20*(2), 166–171. https://doi.org/10.1002/cbic.201800740

Schnaar, R. L., Gerardy-Schahn, R., & Hildebrandt, H. (2014). Sialic acids in the brain: Gangliosides and polysialic acid in nervous system development, stability, disease, and regeneration. *Physiological Reviews*, *94*(2), 461–518. https://doi.org/10.1152/physrev.00033.2013

Scholz, D., Chernyshova, Y., Uckert, A. K., & Leist, M. (2018). Reduced Abeta secretion by human neurons under conditions of strongly increased BACE activity. *Journal of Neurochemistry*, *147*(2), 256–274. https://doi.org/10.1111/jnc.14467

Scholz, D., Pöltl, D., Genewsky, A., Weng, M., Waldmann, T., Schildknecht, S., & Leist, M. (2011). Rapid, complete and large-scale generation of post-mitotic neurons from the human LUHMES cell line. *Journal of Neurochemistry*, *119*(5), 957–971. https://doi.org/10.1111/j.1471-4159.2011.07255.x

Shayman, J. A. (2013). The design and clinical development of inhibitors of glycosphingolipid synthesis: Will invention be the mother of necessity? *Transactions of the American Clinical and Climatological Association*, *124*, 46–60.

Sipione, S., Monyror, J., Galleguillos, D., Steinberg, N., & Kadam, V. (2020). Gangliosides in the brain: Physiology, pathophysiology and therapeutic applications. *Frontiers in Neuroscience*, *14*, 572965. https://doi.org/10.3389/fnins.2020.572965

Stiegler, N. V., Krug, A. K., Matt, F., & Leist, M. (2011). Assessment of chemical-induced impairment of human neurite outgrowth by multiparametric live cell imaging in high-density cultures. *Toxicological Sciences*, *121*(1), 73–87. https://doi.org/10.1093/toxsci/kfr034

van Echten, G., Iber, H., Stotz, H., Takatsuki, A., & Sandhoff, K. (1990). Uncoupling of ganglioside biosynthesis by Brefeldin a. *European Journal of Cell Biology*, *51*(1), 135–139.

Wang, W. X., & Whitehead, S. N. (2020). Imaging mass spectrometry allows for neuroanatomic-specific detection of gangliosides in the healthy and diseased brain. *Analyst*, *145*(7), 2473–2481. https://doi.org/10.1039/c9an02270h

Wratil PR, Horstkorte R, Reutter W (2016) Metabolic Glycoengineering with N-acyl side chain modified Mannosamines. *Angewandte Chemie* (International Ed. in English) *55*(33):9482–512 doi:https://doi.org/10.1002/anie.201601123

Wright, A. J., & Andrews, P. W. (2009). Surface marker antigens in the characterization of human embryonic stem cells. *Stem Cell Research*, *3*(1), 3–11. https://doi.org/10.1016/j.scr.2009.04.001

Yamashita, T., Wu, Y. P., Sandhoff, R., Werth, N., Mizukami, H., Ellis, J. M., Dupree, J. L., Geyer, R., Sandhoff, K., & Proia, R. L. (2005). Interruption of ganglioside synthesis produces central nervous system degeneration and altered axon-glial interactions. *Proceedings of the National Academy of Sciences of the United States of America*, *102*(8), 2725–2730. https://doi.org/10.1073/pnas.0407785102

SUPPORTING INFORMATION

Additional supporting information can be found online in the Supporting Information section at the end of this article.

How to cite this article: Kranaster, P., Blum, J., Dold, J. E. G. A., Wittmann, V., & Leist, M. (2023). Use of metabolic glycoengineering and pharmacological inhibitors to assess lipid and protein sialylation on cells. *Journal of Neurochemistry*, *164*, 481–498. https://doi.org/10.1111/jnc.15737